JOURNAL OF PETROLOGY | VOLUME 43 | NUMBER 10 | PAGES 1857–1883 | 2002

Plume-Associated Ultramafic Magmas of Phanerozoic Age

C. HERZBERG[1]* AND M. J. O'HARA[2]

[1]DEPARTMENT OF GEOLOGICAL SCIENCES, RUTGERS UNIVERSITY, NEW BRUNSWICK, NJ 08903, USA

[2]DEPARTMENT OF EARTH SCIENCES, CARDIFF UNIVERSITY, PO BOX 914, CARDIFF CF10 3YE, UK

RECEIVED FEBRUARY 23, 2001; REVISED TYPESCRIPT ACCEPTED APRIL 1, 2002

A parameterization of experimental data in the 0·2–7·0 GPa pressure range constrains both forward models of potential primary magma compositions that exit the melting regime in the mantle and inverse models for computing the effects of olivine fractionation for any olivine-phyric lava suite. This is used to infer the MgO contents of primary magmas from Gorgona, Hawaii, Baffin Island and West Greenland. They typically contain 18–20% MgO for wide variations in assumed peridotite source compositions, but MgO can drop to 14–17% for Fe-enriched sources, and increase to 24–26% for fractional melts from Gorgona. Primary magmas with 18–20% MgO have potential temperatures of 1520–1570°C. For Gorgona picrites with 24% MgO, the potential temperature and initial melting pressure were about 1700°C and 8·0 GPa, respectively; melting was hot and deep, consistent with the plume model. There are important restrictions to magma mixing in mantle plumes. Primary magmas that exit the melting regime are both well-mixed aggregate fractional melts and isolated fractional melts. The latter can originate from a hot plume axis and be in equilibrium with olivines having mg*-numbers of 93·0–93·6, but they have MgO contents and thermal characteristics that are difficult to constrain.*

KEY WORDS: *komatiite; picrite; basalt; MORB; olivine; mantle plumes; primary magmas; equilibrium melting; accumulated fractional melting*

INTRODUCTION

Mantle plumes are localized regions of hot mantle that are thought to offer ideal opportunities for ultramafic magmatism during the Archaean (Cawthorn, 1975; Fyfe, 1978; Jarvis & Campbell, 1983; Arndt, 1986). However, the importance of ultramafic magmatism is often diminished in models of Phanerozoic hotspot volcanism because basalt eruptives are more common, and the plume model is subject to debate (Anderson, 2000). Even where ultramafic lavas occur, they often have a large olivine phenocryst content and this complicates interpretations of the MgO content of the primary magma. Indeed, the interpretation that picrites can only form by the accumulation of olivine in basaltic liquids (Bowen, 1928) went unchallenged until petrographic evidence demonstrated that skeletal olivine can grow *in situ* in ultrabasic liquids (Drever, 1956; Drever & Johnston, 1957).

Discussions on primary magma compositions are often reduced to the following shortlist of frequently asked questions: How can the composition of a lava flow be used to derive the composition of its primary magma extracted from the melting regime in the mantle? How can an evaluation be made of the effects of olivine fractionation in crust and mantle lithosphere, and the possible sampling of wall-rock olivines from the melting regime? How can we best describe potentially complex fractional melting products of the mantle with equilibrium experimental data? Can the physics of the melt collection process be understood by identifying geochemical differences in the magmatic products of fractional and equilibrium melting? Can inferences be made concerning the extent of melting and crustal thickness from the major element geochemistry of ultramafic lavas? What is the role of heterogeneous mantle? How hot and deep must the melting regime be to produce an ultramafic magma, and can this be used to test the plume model?

Previous discussions of ultramafic rocks have been aggravated by taxonomical confusion over the distinction between picrites and komatiites. For example, we show

*Corresponding author. E-mail: Herzberg@rci.rutgers.edu

in this paper that Cretaceous 'komatiite' lava flows from Gorgona Island and Tertiary 'picrites' from West Greenland crystallized from primary magmas with nearly identical major element compositions and *T–P* conditions of melting. The difference, therefore, is purely textural in that the 'komatiite' flows are spinifex-textured whereas the picrites are generally not. The qualification that komatiites be spinifex-textured (Arndt & Nisbet, 1982) has been dropped with the new IUGS chemical classification (Le Bas, 2000). Nevertheless, discussion continues over the merits of the new classification (Kerr & Arndt, 2001; Le Bas, 2001). As we are concerned mostly with the origin of primary magmas that fit the definitions of both picrite and komatiite, we will use the term 'ultramafic' magma to refer to all magmas with more than 18 wt % MgO.

In previous papers it was shown that Gorgona primary magmas are similar in composition to experimentally constrained anhydrous liquids in equilibrium with harzburgite [L + Ol + Opx] at 3–4 GPa (Herzberg & O'Hara, 1998; Herzberg & Zhang, 1998). Experimental liquid compositions and natural lavas were examined in simplified four-component CMAS space and projected into coordinates defined by olivine, pyroxenes, plagioclase, spinel or garnet. This method of data representation, developed by O'Hara (1968*a*), has the advantage of permitting a simple visual inspection to be made of the full range of analogue magma compositions that can be extracted from the mantle. However, all FeO is combined with MgO in projections, and information is lost in this procedure. Furthermore, the representation of lava compositions in projection is inadequate for distinguishing equilibrium melting from fractional melting processes.

We attempt to provide answers to the above shortlist of frequently asked questions by reporting a new method for constraining the composition of a primary magma for an olivine-phyric lava series. The method involves interfacing projections with diagrams that show absolute weight percentages of FeO and MgO for both equilibrium and fractional melting of various assumed peridotite sources. It differs from the computation of a parental magma using olivine compositions and FeO–MgO exchange coefficients (e.g. Albarède, 1992; Langmuir *et al.*, 1992; Nisbet *et al.*, 1993; Hauri, 1996; Larsen & Pedersen, 2000; Thompson & Gibson, 2000). Parental magmas may not be the same as primary magmas that exit the melting regime owing to modification by olivine crystallization in crustal magma chambers or mantle conduit walls (Larsen & Pedersen, 2000). Our method sees through olivine fractionation effects, and it anticipates potential problems that can arise from the use of olivine phenocrysts or wall-rock xenocrysts with complex fractional melting histories. Indeed, we demonstrate that olivine compositions can provide poor constraints on primary magma MgO content. Model primary magma compositions are used to evaluate the temperatures, pressures and petrological structures of the melting regimes for picrites and komatiites of Phanerozoic age. We show that melting is characteristically hot and deep, consistent with the plume model.

A HYBRID FORWARD AND INVERSE MODEL FOR CALCULATING PRIMARY MAGMA COMPOSITION

The forward component identifies potential primary magma compositions as functions of melt fraction for an assumed peridotite source and melting mechanism. This is done by a parameterization of a large experimental database over a wide pressure range using diagrams of CMAS projections and FeO–MgO. Peridotite compositions that we examine are listed in Table 1. The melting mechanisms that we explore are equilibrium, perfect fractional, and accumulated perfect fractional melting. The inverse component selects a derivative liquid in an erupted lava suite for which olivine fractionation is computed, and this provides an array of possible primary magma compositions. We compare the arrays of potential primary magmas in both forward and inverse models, and make use of model melt fractions in the forward component to seek a unique primary magma solution. Model solutions provide primary magma composition, melt fraction, residuum mineralogy, and temperature of eruption and melt collection in the melting regime. Computed primary magma compositions depend on assumptions concerning peridotite source composition and melting mechanism, and we evaluate these effects in the forward model component.

MAGMAS IN PROJECTION

The compositions of magmas formed by equilibrium melting of mantle peridotite are shown in projection in Fig. 1a and b. These projections are based on experiments in the system CaO–MgO–Al_2O_3–SiO_2 summarized by Herzberg & O'Hara (1998). Other components such as TiO_2, Cr_2O_3, FeO, MnO, Na_2O, K_2O and NiO can expand and contract liquidus crystallization fields to varying degrees. The replacement of MgO by FeO does little to change the projected locations of the cotectics and invariant points, but the effects of TiO_2, Na_2O and K_2O are more substantial. Cotectic shifts have been evaluated in the projection code by optimizing the match to the phase equilibria in the system CaO–MgO–Al_2O_3–SiO_2 (Herzberg & O'Hara, 1998). A description of the projection code is given in Electronic Appendix 1, which may be downloaded from the

Table 1: Fertile and depleted peridotite compositions

	Kettle R[1]	Kettle R[2]	Abyssal[3]	Average[4]	MM3[5]	1611[6]	1611	Fe peridotite[7]
SiO_2	44·90	44·90	44·55	44·29	45·50	43·70	44·55	44·69
TiO_2	0·16	0·16	0·04	0·09	0·11	0·25	0·25	0·16
Al_2O_3	4·26	4·26	2·36	2·36	3·98	2·75	2·80	4·24
Cr_2O_3	0·41	0·41	0·41	0·43	0·68	0·28	0·28	0·41
Fe_2O_3	n.a.	n.a.	0·20*	0·20*	n.a.	n.a.	n.a.	n.a.
FeO	8·02	8·02	8·07	8·13	7·18	10·05	10·25	9·04
MnO	0·13	0·13	0·14	0·13	0·13	0·13	0·13	0·13
MgO	37·30	38·12	41·80	41·64	38·30	37·22	37·94	37·35
CaO	3·45	3·45	2·14	2·20	3·57	3·26	3·32	3·43
Na_2O	0·22	0·22	0·05	0·23	0·31	0·33	0·34	0·22
K_2O	0·09	0·09	n.a.	0·04	0·01	0·14	0·14	0·09
NiO	0·24	0·25	0·24	0·27	0·23	n.a.	n.a.	0·24
Sum	99·18	100·00	100·00	100·00	100·00	98·25	100·00	100·00
mg-no.	89·2	89·4	90·2	90·1	90·5	86·8	86·8	88·0

Analyses in wt % oxides. [1]KR-4003 Kettle River Peridotite (Walter, 1998). [2]Walter composition with MgO raised to total 100 (used in calculations in this work; see text). [3]Abyssal peridotite RC27-9-30 of Baker & Beckett (1999). [4]Average mantle peridotite (590 analyses; Herzberg, 1993). [5]MM3 from Baker & Stolper (1994). [6]PHN1611 from Kushiro (1996). [7]Model Fe-rich peridotite = KR-4003 + FeO − MgO (see text). *Fe_2O_3 calculated from Canil *et al.* (1994). n.a., not analysed.

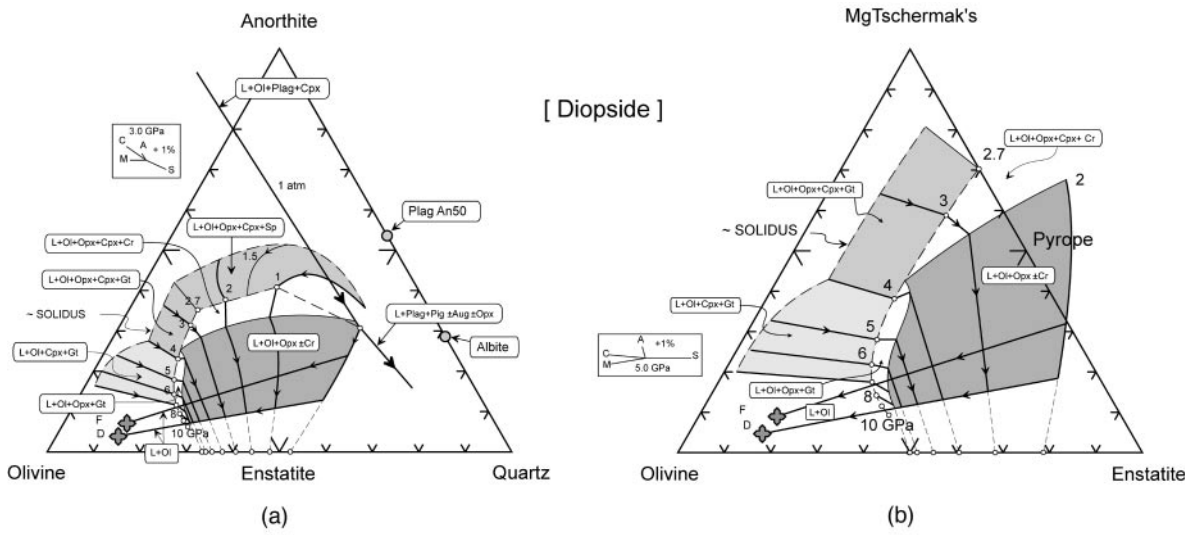

Fig. 1. (a) Projection of compositions (mole percent) of liquids in equilibrium with mantle peridotite from Diopside (CMS_2) and $Na_2O{\cdot}Si_3O_6$ and $K_2O{\cdot}Si_3O_6$ into the plane Olivine (M_2S)–Anorthite (CAS_2)–Silica (S), modified from Herzberg & O'Hara (1998). F, Fertile mantle peridotite (KR-4003; Table 1); D, depleted mantle peridotite (abyssal; Table 1). Phase assemblages are indicated by labels. L, Liquid; Ol, Olivine; Opx, Orthopyroxene; Cpx, Clinopyroxene; Gt, Garnet; Sp, Spinel; Cr, Chromite (see text). Fine continuous lines with arrows indicate cotectic equilibria at the pressures shown (GPa); arrows point up-temperature in the sense of advanced partial melting. Bold continuous lines with large arrows indicate cotectics at 1 atm; arrows point down-temperature in the sense of progressive partial crystallization. Inset shows the effect of adding 1 wt % of CaO, MgO, Al_2O_3 and SiO_2 to the compositions of liquids at the invariant points at the pressures indicated. Projection code for combining all oxide components to CMAS equivalents has been given by Herzberg & O'Hara (1998) and in Electronic Appendix 1. (b) Projection of compositions (mole percent) of liquids in equilibrium with mantle peridotite from Diopside (CMS_2) and $Na_2O{\cdot}Si_3O_6$ and $K_2O{\cdot}Si_3O_6$ into the plane Olivine (M_2S)–MgTschermak's (MAS)–Enstatite (M_2S_2), modified from Herzberg & O'Hara (1998). Symbols as for (a).

Journal of Petrology Web site at http://www.petrology.oupjournals.org. A CMAS description of mantle melting reduces the system SiO_2–TiO_2–Al_2O_3–Cr_2O_3–FeO–MnO–MgO–CaO–Na_2O–K_2O–NiO to four 'equivalent' components in CaO–MgO–Al_2O_3–SiO_2. The experimental database used in the construction of these projections was listed by Herzberg & O'Hara (1998), and is here upgraded with new data at pressures from 1 to 2·7 GPa (Falloon *et al.*, 1999*a*, 1999*b*; Gudfinnsson & Presnall, 2000), previously published data that we had overlooked (Kushiro, 1996) and the experimental results of Walter (1998). A preliminary draft of Walter's initial results was made available to the first author, and these were encorporated into the projections of Herzberg & O'Hara (1998). The final set of experimental results that were published by Walter (1998) differed somewhat in that only superior data were included, those being data for which an optimum mass balance was demonstrated. Data of Kinzler (1997) have not been used because totals in many reported liquid compositions are low (i.e. 97–99%), and high pressures arise as an artefact of low SiO_2.

The new projections in Fig. 1 are very similar to those reported by Herzberg & O'Hara (1998), differing mainly in a more precise location of the harzburgite cotectics [L + Ol + Opx] at 3 and 4 GPa. In most cases the revised harzburgite cotectics at 2–6 GPa describe the experimental data to within ±0·5 GPa (Herzberg & O'Hara, 1998). Experimental picritic liquid compositions reported by Longhi (1995) exhibit model pressures in projection that are typically 0·5 GPa higher than his experimental nominal pressures, a difference that points to uncertainties associated with pressure calibrations (Herzberg *et al.*, 2000; Hirschmann, 2000). The 1 GPa cotectics for lherzolite [L + Ol + Opx + Cpx ± Spinel ± Chromite) and harzburgite [L + Ol + Opx ± Chromite) shown in Fig. 1a describe data for a wide range of compositions to within ±0·2 GPa (Hirose & Kushiro, 1993; Baker & Stolper, 1994; Baker *et al.*, 1995; Kushiro, 1996; Hirschmann *et al.*, 1998; Falloon *et al.*, 1999*a*).

The phase relations shown in Fig. 1a and b apply to equilibrium melting of a fertile and a depleted mantle peridotite (Table 1). The fertile peridotite is a xenolith from Kettle River, British Columbia (KR-4003; Xue *et al.*, 1990; Walter, 1998), and the depleted composition is a sample of abyssal peridotite (Baker & Beckett, 1999). Oxides in KR-4003 sum to 99·18 (Xue *et al.*, 1990), and we suspect that this arises from low MgO (Table 1); liquids analysed by Walter (1998) in experiments on this sample containing only liquid + olivine are better described with a bulk composition having 38·12% MgO rather than 37·3% MgO (Table 1). Liquids in low-variance assemblages such as spinel-lherzolite [L + Ol + Opx + Cpx + Sp] project along common cotectics. Differences can arise, however, for liquids in equilibrium with olivine [L + Ol] and harzburgite [L + Ol + Opx] near the melting out of Opx owing to the differences in bulk composition (Fig. 1).

The experimental data of O'Hara *et al.* (1971) and Walter (1998) are consistent with a 2·7 GPa pressure for the transformation of spinel to garnet peridotite (Herzberg *et al.*, 2000). This pressure defines an important break in the pressure-induced track of liquids formed by initial melting of mantle peridotite (Fig. 1a). At higher pressures, liquids in equilibrium with garnet peridotite become substantially enriched in MgO and depleted in Al_2O_3 (see also Herzberg, 1992). At pressures between 3·0 and 4·0 GPa, initial melts of fertile peridotite KR-4003 are in equilibrium with Opx (L + Ol + Opx + Cpx + Gt; Walter, 1998). At pressures between 4·0 and 4·5 GPa, initial melts of KR-4003 are produced from the Opx-free assemblage [L + Ol + Cpx + Gt] owing to the stabilization of subcalcic clinopyroxene (Walter, 1998). When Opx becomes unstable, liquids on the solidus must have lower SiO_2 than those in equilibrium with Opx because of the reaction Ol + Cpx + Gt = L + Opx (e.g. Herzberg & Zhang, 1998; Walter, 1998).

CALCULATED MAGMA COMPOSITIONS: BALANCE OF MgO AND FeO IN MAGMAS, SOURCES AND RESIDUES

Partition and exchange coefficients

The procedure of Beattie *et al.* (1991) and Jones (1995) has been adopted for computing the compositions of olivine and orthopyroxene in equilibrium with a liquid of a known composition. The liquid composition in weight percent oxides is first recalculated to mole percent oxides, and the compositions of olivine and orthopyroxene are computed using the molecular percent partition coefficients:

$$D_i^{Ol/L} = X_i^{Ol}/X_i^{L} \quad (1)$$

and

$$D_i^{Opx/L} = X_i^{Opx}/X_i^{L} \quad (2)$$

where X_i refers to the mole fraction of oxide component i in the phases liquid (L), olivine (Ol) and orthopyroxene (Opx). Beattie *et al.* (1991) and Jones (1995) showed that D_i values for some components are often dependent on the partitioning of MgO between mineral and liquid, so that

$$D_i^{Ol/L} = A_i^{Ol/L} D_{MgO}{}^{Ol/L} + B_i^{Ol/L} \quad (3)$$

and

Table 2: Olivine liquid distribution coefficients (molar)

Oxide	*D*(Olivine/Liquid)	1σ	*n*
TiO_2	0·03	0·020	70
$AlO_{1,5}$	$[-0{\cdot}031 + 0{\cdot}0035D_{MgO} + 0{\cdot}093/D_{MgO})$	0·004	140
$CrO_{1,5}$	$[0{\cdot}183 + 0{\cdot}067D_{MgO}]$	0·260	117
$FeO_{1,5}$	0		
FeO	see text		
MnO	$[0{\cdot}118 + 0{\cdot}214D_{MgO}]$	0·360	143
CaO	$[-0{\cdot}019 + 0{\cdot}007D_{MgO} + 0{\cdot}063/D_{MgO}]$	0·007	212
$NaO_{0·5}$	0		
$KO_{0·5}$	0		
NiO*	$[-3{\cdot}665 + 3{\cdot}346D_{MgO}]$		

*From Beattie *et al.* (1991). *n*, number of experimental data points used in regression. $D_{MgO} = X_{MgO}^{Ol}/X_{MgO}^{Liquid}$.

Table 3: Orthopyroxene–liquid distribution coefficients (molar)

Oxide	*D*(Orthopyroxene/Liquid)	1σ	*n*
TiO_2	$[0{\cdot}004 + 0{\cdot}065D_{MgO}]$	0·06	93
$AlO_{1·5}$	$[-2{\cdot}61 + 17{\cdot}57\ X_{SiO_2} - 24{\cdot}93\ X_{SiO_2}]$*	0·05	31
$CrO_{1·5}$	$[-0{\cdot}67 + 0{\cdot}049D_{MgO} + 0{\cdot}753D^2_{MgO}]$	1·83	76
$FeO_{1·5}$†	0·3		
FeO	see text		
MnO	$[0{\cdot}14 + 0{\cdot}274D_{MgO}]$	0·27	72
CaO	$[-0{\cdot}28 + 0{\cdot}1D_{MgO} + 0{\cdot}55/D_{MgO}]$	0·03	100
$NaO_{0·5}$	0·1	0·03	109
$KO_{0·5}$	0		
NiO‡	$[-0{\cdot}263 + 1{\cdot}206D_{MgO}]$		

*Ol + Opx assemblages only.
†Estimated to match measured Fe_2O_3 (Canil *et al.*, 1994).
‡From Beattie *et al.* (1991).
n, number of experimental data points used in regression; $D_{MgO} = X_{MgO}^{Opx}/X_{MgO}^{Liquid}$.

$$D_i^{Opx/L} = A_i^{Opx/L} D_{MgO}^{Opx/L} + B_i^{Opx/L} \quad (4)$$

where and A_i and B_i are constants for each oxide component i.

We have added to and re-evaluated the constants A_i and B_i of Beattie *et al.* (1991) and Jones (1995) for TiO_2, Al_2O_3, Cr_2O_3, Fe_2O_3, MnO, CaO, Na_2O and K_2O, using experimental data described in Electronic Appendix 2 (available from the *Journal of Petrology* Web site at http://www.petrology.oupjournals.org). Results are listed in Tables 2 and 3. For the partitioning of Fe_2O_3, $D_{Fe_2O_3}^{Ol/L} = 0$, and $D_{Fe_2O_3}^{Opx/L} = 0{\cdot}3$; this partition coefficient for Opx/Liquid yields $Fe^{3+}/\Sigma Fe = 0{\cdot}06$ as observed in orthopyroxenes from a wide range of peridotites (Canil *et al.*, 1994). For the partitioning of FeO, $A_{FeO}^{Ol/L}$ and $A_{FeO}^{Opx/L}$ are equivalent to the exchange coefficients

$$K_D^{Ol/L}{}_{FeO/MgO} = D_{FeO}^{Ol/L}/D_{MgO}^{Ol/L} \quad (6)$$

and

$$K_{DOpx/L}^{FeO/MgO} = D_{FeO}^{Opx/L}/D_{MgO}^{Opx/L}. \quad (7)$$

Roeder & Emslie (1970) determined the exchange coefficient for olivine to be $0{\cdot}30 \pm 0{\cdot}03$ for basaltic liquids with about 8% MgO at 1 atm, a value that is commonly used in petrological modelling. This is observed again in Fig. 2 with our database, but it can also be seen that $K_D^{Ol/L}{}_{FeO/MgO}$ increases to 0·35–0·36 for liquids with MgO >20%. Clearly, the values of A_{FeO} in equations (3) and (4) are not constant. Experimental data shown in Fig. 2 have been regressed with the equations

$$K_D^{Ol/L}{}_{FeO/MgO} = 0{\cdot}381 - 0{\cdot}790/MgO + 1{\cdot}039/MgO^2 \quad (8)$$

where MgO is the weight percent concentration in the liquid and

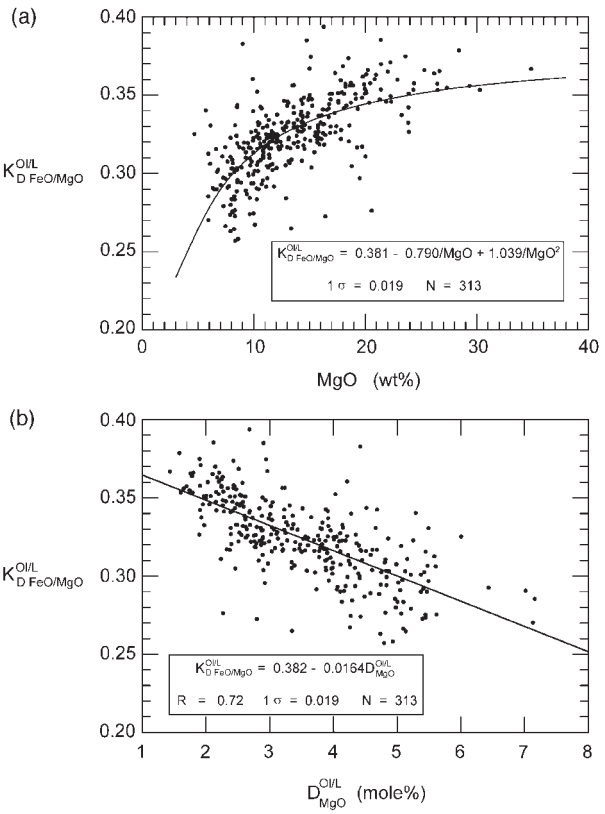

Fig. 2. (a, b) Exchange coefficient K_D for FeO and MgO between olivine and liquid as a function of composition of the liquid and the partition coefficient for MgO between olivine and liquid. Data sources are cited in Electronic Appendix 2.

$$K_D^{Ol/L}{}_{FeO/MgO} = 0{\cdot}382 - 0{\cdot}0164 D_{MgO}^{Ol/L} \quad (9)$$

where $D_{MgO}^{Ol/L}$ is the distribution of MgO between olivine and liquid, on a molecular basis. A regression of experimental data for orthopyroxene–liquid yields

$$K_D^{Opx/L}{}_{FeO/MgO} = 0{\cdot}384 - 0{\cdot}035 D_{MgO}^{Opx/L}. \quad (10)$$

The uncertainty in calculating $K_D^{Ol/L}{}_{FeO/MgO}$ from equations (8) and (9) is $\pm 0{\cdot}019$ at the 1σ level, compared with an uncertainty of $\pm 0{\cdot}011$ (1σ) that arises strictly from errors in the analysis of olivine and glass using the electron microprobe. Uncertainties arising from Fe_2O_3 should be small because experimental samples were encapsulated in either carbon or metallic iron, as discussed in Electronic Appendix 2. The difference between $\pm 0{\cdot}019$ and $\pm 0{\cdot}011$ is fairly small, and most of it is likely to arise from temperature and pressure effects (Takahashi & Kushiro, 1983; Ulmer, 1989; Sobolev & Danyushevsky, 1994). Indeed, we observe positive correlations of $K_D^{Ol/L}$ with temperature and pressure. However, regressions of $K_D^{Ol/L}$ vs pressure and temperature yield 1σ uncertainties of $\pm 0{\cdot}024$ (correlation coefficient $R = 0{\cdot}46$) and $\pm 0{\cdot}021$ ($R = 0{\cdot}60$), respectively, larger than standard deviations for $K_D^{Ol/L}$ vs liquid MgO content ($\pm 0{\cdot}019$; $R = 0{\cdot}69$). Values of $K_D^{Ol/L}$ estimated from equations (8) and (9) are significantly lower than those of Ulmer (1989). For example, both experiments reported by Walter (1998) and our regression in Fig. 2 yield $K_D^{Ol/L} = 0{\cdot}34$–$0{\cdot}36$ for liquids equilibrated at 3·0–7·0 GPa, whereas Ulmer (1989) predicted 0·38–0·51. We have not attempted to resolve the independent effects of temperature, pressure and composition on $K_D^{Ol/L}$ for several reasons. First, it is difficult to do so with confidence because the MgO content of the liquid is highest in experiments conducted at elevated temperatures and pressures. Second, our method of calculating $K_D^{Ol/L}$ from liquid composition has the advantage of considerable simplicity because it does not require an independent way of evaluating pressure.

The fraction of sites available for Fe^{2+} and Mg is 0·667 and 0·5 for olivine and orthopyroxene, respectively. These are filled with Mn, Ca, Na, K and Ni; Ti is partitioned exclusively into the tetrahedral sites; Al and Cr are distributed equally between tetrahedral and octrahedral sites to maintain charge balance. The remaining octahedral sites are filled with Fe^{2+} and Mg, calculated by rearranging equations (6) and (7) to

$$K_D^{Ol/L}{}_{FeO/MgO} = (FeO/MgO)^{Ol}/(FeO/MgO)^{L} \quad (11)$$

and

$$K_D^{Opx/L}{}_{FeO/MgO} = (FeO/MgO)^{Opx}/(FeO/MgO)^{L} \quad (12)$$

with solutions from equations (9) and (10). Olivine and orthopyroxene compositions are then converted from mole percent to weight percent. A computer program is provided in Electronic Appendix 2 for computing the weight percent composition of olivine and orthopyroxene in equilibrium with a liquid of a known composition.

Effect of H_2O on exchange coefficients

Ulmer's (1989) FeO–MgO exchange coefficients for experimentally equilibrated olivine–liquid pairs were for starting material compositions that contained 1·98–3·28 wt % H_2O. These hydrous data can be reproduced to within $\pm 0{\cdot}023$ (1σ) using equations (8) and (9) for anhydrous data, indicating that H_2O has little effect on $K_D^{Ol/L}{}_{FeO/MgO}$.

Liquids in equilibrium with olivine and harzburgite

The compositions of liquids in equilibrium with olivine [L + Ol] and harzburgite [L + Ol + Opx] were computed by mass balance solutions to the equilibrium melting equation

$$C_L = C_o / [F(1-D) + D] \quad (13)$$

where C_L is the weight percent of an oxide component in the liquid phase, C_o is the initial oxide concentration in the peridotite source composition of interest (Table 1), F is the melt fraction, and D is the bulk distribution coefficient applicable at any chosen value of F.

The bulk distribution coefficient is the concentration of the oxide component in the multiphase residue divided by the concentration in the liquid, and takes the form

$$D = C_S / C_L. \quad (14)$$

D is determined from

$$D = X_{Ol} D^i_{Ol} + X_{Opx} D^i_{Opx} \quad (15)$$

where X_{Ol} and X_{Opx} are the weight proportions of olivine and orthopyroxene in the residue, and D^i_{Ol} and D^i_{Opx} are the weight percent olivine–liquid and orthopyroxene–liquid partition coefficients, respectively. We distinguish weight percent partition coefficients from molecular percent partition coefficients with D^i_{Ol} and D_i^{Ol}, respectively. The weight percent partition coefficients have been calculated by computing the weight percent composition of olivine and orthoproxene in equilibrium with the melt, as discussed above, weighted with equation (15) according to the proportions of olivine and orthopyroxene in the residue.

Coexisting liquid and crystalline compositions were solved with equation (13) using an iterative procedure that incrementally varies F from 1·0 to a value that is regulated by the stability of clinopyroxene. Liquid compositions in equilibrium with olivine (L + Ol) are

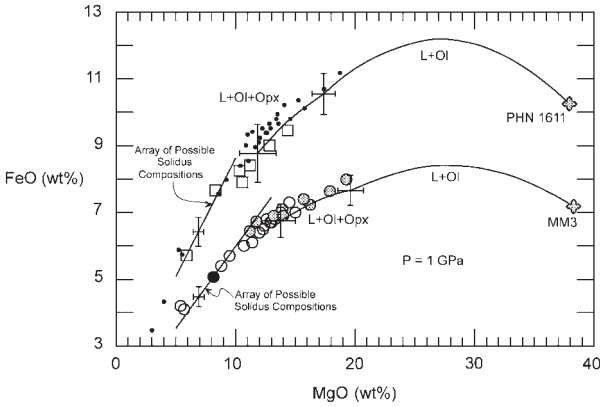

Fig. 3. Experimental and calculated FeO and MgO contents of liquids in equilibrium with peridotite at 1 GPa. Experimental data: ○, data of Hirschmann *et al.* (1998) on peridotite MM3; grey circles, data of Falloon *et al.* (1999*a*) on peridotite MM3; ●, liquid composition at the solidus suggested by Falloon *et al.* (1999*a*); □, data of Kushiro (1996) on peridotite PHN1611; •, liquids calculated using equations (16) and (17) in the text. Calculated liquids: curved lines indicate FeO and MgO for [L + Ol] and [L + Ol + Opx]; straight lines indicate FeO and MgO on the solidus calculated for olivines with *mg*-number = 86·9 for PHN1611 (Smith & Boyd, 1987) and *mg*-number = 90·6 for MM3 (Baker & Stolper, 1994). Uncertainties in calculated FeO and MgO contents arise from $\pm 1\sigma$ $K_D^{Ol/L}{}_{FeO/MgO}$.

solved for $X_{Opx} = 0$, and liquid compositions in equilibrium with harzburgite (L + Ol + Opx) are solved for $X_{Opx} = 0$ to a value that is also regulated by the stability of clinopyroxene (L + Ol + Opx + Cpx). Clinopyroxene stability is constrained experimentally in Fig. 1, into which computed liquid compositions are projected. Harzburgite cotectics in Fig. 1 at 1–6 GPa constrain the pressure for projected liquid compositions. For example, in the case of equilibrium melting of fertile mantle peridotite KR-4003 (Table 1), Cpx melts out when F reaches 0·23 at 1·0 GPa, similar to that for other fertile compositions (Langmuir *et al.*, 1992; Baker & Stolper, 1994). The effect of pressure is to increase F at which Cpx remains stable, and this is shown in more detail below.

The contents of FeO and MgO in liquids equilibrated with olivine and harzburgite residua at 1 GPa have been calculated for peridotite compositions PHN1611 (Kushiro, 1996) and MM3 (Hirschmann *et al.*, 1998; Falloon *et al.*, 1999*a*), and the results are shown in Fig. 3. The calculated compositions agree well with the experimentally observed liquids, and are consistently within the uncertainties associated with both the location of the harzburgite cotectic (Fig. 1a; $\pm 0{\cdot}2$ GPa) and $K_D^{Ol/L}$ (Fig. 2; $\pm 0{\cdot}019$ at the 1σ level). Peridotite 1611 is considerably more FeO-rich than MM3 (Table 1), and this propagates to the partial melt products in a predictable way. Indeed, it is possible to independently compute the liquid compositions of PHN1611 from those for MM3. This can be done by the approximations

$$C_{L\ FeO,\ PHN1611} \cong C_{L\ FeO,\ MM3}(C_{o\ FeO,\ PHN1611})/(C_{o\ FeO,\ MM3}) \quad (16)$$

and

$$C_{L\ MgO,\ PHN1611} \cong C_{L\ MgO,\ MM3}(C_{o\ MgO,\ PHN1611})/(C_{o\ MgO,\ MM3}). \quad (17)$$

The approximations arise because D values for PHN1611 are not the same as D values for MM3 at a given melt fraction F. Nevertheless, the compositions of liquids formed by equilibrium melting of PHN1611 calculated by these different methods agree very well with the experimentally observed compositions (Fig. 3). We therefore have independent ways of evaluating the FeO and MgO contents of liquids formed by partial melting of a peridotite composition for which no experimental data are available.

Liquids on the solidus

We can constrain the compositions of liquids that form immediately on the solidus where $F \rightarrow 0$ by combining equations (8) and (11):

$$(FeO/MgO)^{Ol}/(FeO/MgO)^{L} = 0{\cdot}381 - 0{\cdot}790/MgO + 1039/MgO^2 \quad (18)$$

where MgO and FeO for olivine and liquid are weight percent oxides. This is done by solving for FeO^L for an array of possible values for MgO^L on the solidus, given that $(FeO/MgO)^{Ol}$ is known for the unmelted peridotite (Smith & Boyd, 1987; Baker & Stolper, 1994). Results are shown in Fig. 3.

A forward model for equilibrium melting of a fertile peridotite source (FeO ~8·0%)

A computation has been made of contents of SiO_2, TiO_2, Al_2O_3, Cr_2O_3, FeO, MnO, MgO, CaO, Na_2O, K_2O and NiO for magmas produced by equilibrium melting of a fertile peridotite source with 8·0% FeO (Table 1; KR-4003) at pressures that range from 1 to 6 GPa. Results for FeO and MgO are shown in Fig. 4a and representative model liquid compositions are listed in Table A1 of Electronic Appendix 3 on the *Journal of Petrology* Web site at http://www.petrology.oupjournals.org. Liquids were computed for olivine [L + Ol] and harzburgite [L + Ol + Opx] assemblages by the method discussed above, and for liquids immediately on the solidus. Uncertainties arising from 1σ in $K_D^{Ol/L}{}_{FeO/MgO}$ are typically $\pm 1{\cdot}4\%$ MgO and $\pm 0{\cdot}52\%$ FeO, and propagate to an uncertainty of $\pm 1{\cdot}5$ GPa where isobaric cotectics are compressed in FeO–MgO space (Fig. 4a).

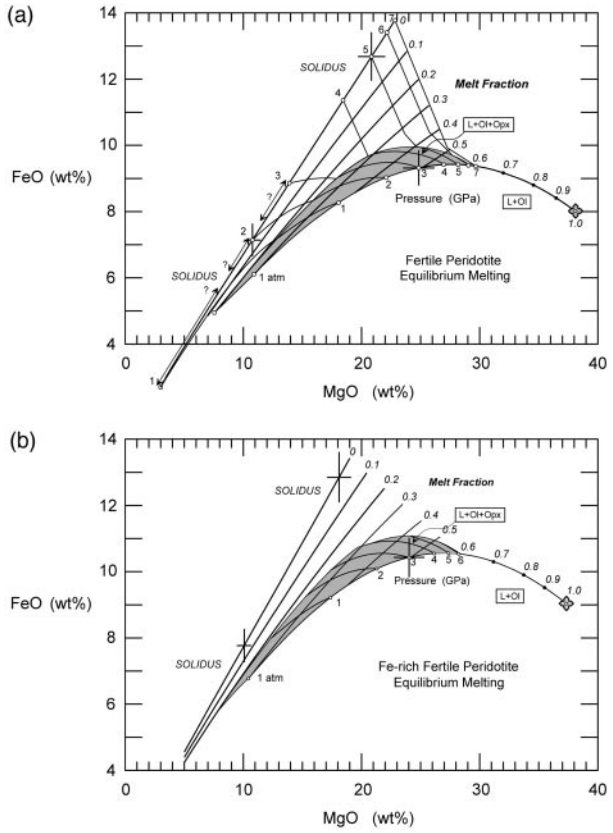

Fig. 4. (a) FeO and MgO contents of liquids formed by isobaric equilibrium melting of fertile mantle peridotite KR-4003 (Table 1). FeO–MgO–F systematics are computed from equations (21)–(23) in the text. Liquids in equilibrium with olivine [L + Ol] and harzburgite [L + Ol + Opx] are computed from equations (13)–(15) and Fig. 1 (see text). Crosses indicate uncertainties in calculated FeO and MgO contents arise from $\pm 1\sigma$ $K_D^{Ol/L}{}_{FeO/MgO}$. Arrows along solidus at 1, 2, and 3 GPa indicate uncertainties from experimental data on PHN-1611 and MM3 and their propagation to KR-4003 (see text for discussion). Representative liquid compositions are given in Electronic Appendix 1 (Table A1). Phase assemblages between those for the solidus and harzburgite [L + Ol + Opx] are not shown for clarity, but include the following from Fig. 1a and b: [L + Ol + Opx + Cpx + Sp], [L + Ol + Opx + Cpx + Cr], [L + Ol + Opx + Cpx + Gt], [L + Ol + Cpx + Gt], [L + Ol + Opx + Gt]. (b) FeO and MgO contents of liquids formed by equilibrium melting of Fe-rich fertile mantle peridotite (Table 1). FeO–MgO–F systematics are computed from equations (21)–(23) given in the text. Liquids in equilibrium with olivine [L + Ol] and harzburgite [L + Ol + Opx] are computed from equations (13)–(15) and Fig. 1 (see text). Crosses indicate uncertainties in calculated FeO and MgO contents arising from $\pm 1\sigma$ $K_D^{Ol/L}{}_{FeO/MgO}$.

Liquids immediately on the anhydrous solidus were computed from equation (18) and the composition of subsolidus olivine, which has an *mg*-number of 89·5 (Walter, 1998; olivine analysis 60·02). The array of permissible solutions for FeO and MgO in liquids in equilibrium with this composition of olivine at the solidus is accurately defined (Fig. 4a), but difficulties arise in calibrating this array for pressure. For example, in the absence of any experimental data, the FeO and MgO contents of the first drop of liquid on the solidus at 4 GPa could be located anywhere on the solidus array.

Ironically, liquids on the solidus at 4–7 GPa may be better known than those at 1–3 GPa. The data of Walter (1998) show that FeO and MgO are negatively correlated and linear for [L + Ol + Cpx + Gt] at 6 and 7 GPa and for F ranging from 0·11 to 0·41. These isobaric FeO–MgO arrays are nearly orthogonal to the solidus array, which is intersected at well-defined points (Fig. 4a). Liquids on the solidus at 1 and 3 GPa were constrained by factoring liquid compositions for MM3 and PHN1611 according to bulk composition, as discussed above (Fig. 3). At 1 GPa the FeO and MgO contents of liquids at F in the 0–0·20 range nearly parallel those on the solidus FeO–MgO array (Figs 3 and 4a). For a basalt with 12% MgO, a $\pm 1\sigma$ uncertainty in $K_D^{Ol/L}{}_{FeO/MgO}$ propagates to FeO contents at 1 GPa that cannot be statistically distinguished from those at 2 GPa. It is therefore understandable that disagreement exists over the FeO and MgO contents of the near-solidus liquid at 1 GPa for peridotite MM3 (Baker & Stolper, 1994; Baker *et al.*, 1995; Hirschmann *et al.*, 1998; Falloon *et al.*, 1999*a*). The positions of the model isobaric cotectics between the solidus and harzburgite saturation shown in Fig. 4a usually differ from experimental determinations by no more than $\pm 0{\cdot}5$ GPa. However, this uncertainty can increase to $\pm 1{\cdot}5$ GPa where the isobaric cotectics are compressed in FeO and MgO space, similar to those for [L + Ol + Opx]. In most cases, the model FeO–MgO isobaric cotectics agree with experimental cotectics to within ± 1 GPa in the 1–7 GPa range and therefore pressure information cannot be accurately obtained for natural lava compositions. We believe that a ± 1 GPa uncertainty is a problem that is common to all petrological models that operate within the $\pm 0{\cdot}019$ bound of uncertainty in $K_D^{Ol/L}{}_{FeO/MgO}$.

A forward model for equilibrium melting of an Fe-rich fertile peridotite source (FeO ~9·0%)

We now examine the consequences of partial melting of a peridotite source that is enriched in FeO. The average of 590 samples of peridotite from off-craton occurrences contains 8·14% and this varies by $\pm 0{\cdot}90$% FeO at the 1σ level (Herzberg, 1993). Most peridotites from ocean basins and xenoliths display wide variations in MgO content at ~8·0% FeO, and they display no relationship between FeO and indicators of fertility or depletion (e.g. TiO_2, Al_2O_3, Na_2O; Herzberg, 1993; Baker & Beckett, 1999; Griffin *et al.*, 1999; excluding cratonic mantle). Calculations have been performed on a synthetic composition formed from Kettle River peridotite KR-4003

by a simple replacement of MgO with FeO. This Fe-rich source contains 9·04% FeO (Table 1), which is higher than the average FeO content by 1σ (i.e. 8·14 + 0·90), and it is identically located in projection with its precursor, KR-4003.

Shown in Fig. 4b are the compositions of liquids formed by equilibrium melting of this Fe-rich fertile source with residual harzburgite and olivine. These liquids are elevated in FeO compared with normal fertile peridotite with about 8% FeO, a result that is intuitively obvious. Indeed, liquids are elevated in FeO by about 0·9% at most pressures, an amount that corresponds to enrichment of normal mantle with 0·9% FeO. We do not provide pressure information for compositions on the solidus or between the solidus and harzburgite-saturated assemblages because we have no experimental data for pressures in the 2–6 GPa range.

A forward model for equilibrium melting of a depleted peridotite source (FeO ~8·0%)

The depleted peridotite sample chosen for this forward model is an abyssal peridotite from Baker & Beckett (1999). Inspection of Table 1 shows that it has nearly the same composition as the average of 590 mantle peridotite samples from off-craton occurrences (Herzberg, 1993). This depleted source contains about 42% MgO and 8% FeO, similar to FeO in fertile peridotite.

Shown in Fig. 5a are the compositions of liquids formed by equilibrium melting of this depleted source with residual harzburgite and olivine. Again, we do not provide pressure information owing to a lack of experimental data. The compositions shown for olivine- and harzburgite-saturated assemblages are compared with those for equilibrium melting of fertile peridotite in Fig. 5b. In the 1 atm to 2 GPa pressure range, there is a similarity in FeO and MgO contents of harzburgite-equilibrated liquids for fertile and depleted sources having 8·0% FeO. However, at 3–5 GPa, harzburgite-equilibrated liquids of a depleted source with 8·0% FeO are similar in FeO and MgO to those for Fe-rich fertile peridotite with 9·0% FeO. These observations illustrate the harzards that can result from using the composition of an erupted magma to infer the FeO content of a peridotite source.

FeO–MgO–F systematics for all forward models of equilibrium melting

It is sometimes convenient to consider a residue–liquid equilibrium rather than an olivine–liquid equilibrium, although both are obviously identical when olivine is the only residuum phase. If the *mg*-number of a residue is nearly identical to that of olivine in that residue, then equation (18) can be modified so that $(FeO/MgO)^{Ol}$ is

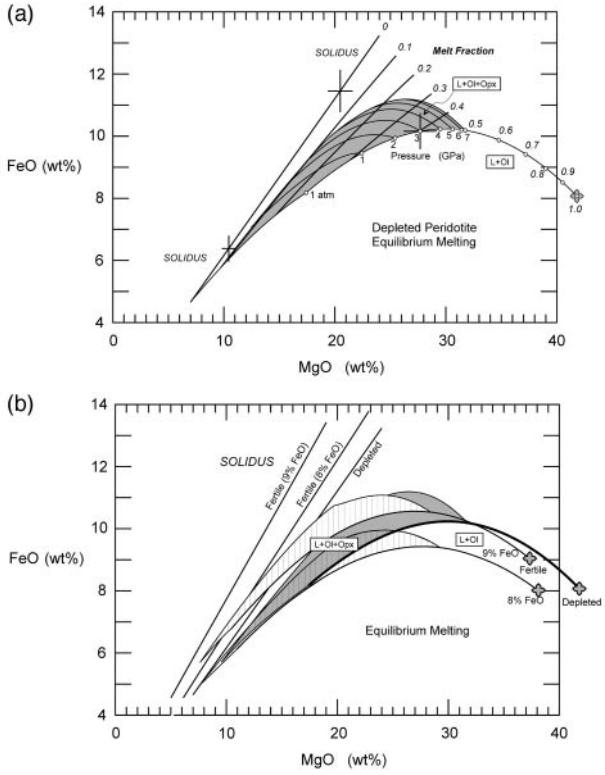

Fig. 5. (a) FeO and MgO contents of liquids formed by equilibrium melting of depleted mantle peridotite (Table 1). FeO–MgO–F systematics are computed from equations (21)–(23) given in the text. Liquids in equilibrium with olivine [L + Ol] and harzburgite [L + Ol + Opx] are computed from equations (13)–(15) and Fig. 1 (see text). Crosses indicate uncertainties in calculated FeO and MgO contents arising from $\pm 1\sigma$ $K_D^{Ol/L}{}_{FeO/MgO}$. (b) A comparison of FeO and MgO contents of liquids formed by equilibrium melting of various peridotite source compositions.

replaced by $(FeO/MgO)_o$, the initial source rock composition. Indeed, the arrays of FeO and MgO we compute for liquids on the solidus using source rock composition are nearly identical to those computed using olivine in equation (18), the difference being <0·1% FeO. The equation for the exchange coefficient can therefore be generalized as

$$K_D^{S/L}{}_{FeO/MgO} \cong K_D^{Ol/L}{}_{FeO/MgO} \quad (19)$$

where S refers to the solid residue. For fertile peridotite KR-4003 shown in Fig. 4a, we have obtained FeO and MgO contents for the residue compositions from the mass balance equation

$$C_o = FC_L + (1-F)C_S \quad (20)$$

where C_S refers to the residue composition. A regression yields

$$K_D^{S/L}{}_{FeO/MgO} = 0{\cdot}381 - 0{\cdot}774/MgO_L + 0{\cdot}998/MgO_L{}^2 \quad (21)$$

where MgO_L refers to the weight percent MgO in the

liquid. Solutions to equations (8) and (21) yield olivine–liquid and residue–liquid exchange coefficients that are almost identical. The batch melting equation (13) can be solved for any melt fraction F:

$$FeO_L = FeO_o / [F(1 - D_{FeO}) + D_{FeO}] \quad (22)$$

by combining it with the equation for mass balance to yield

$$D_{FeO} = (MgO_o - F MgO_L) K_D^{S/L}{}_{FeO/MgO} / [(1 - F) MgO_L] \quad (23)$$

where FeO_o and MgO_o are the weight percent FeO and MgO in the peridotite source. Equations (21), (22) and (23) yield general solutions to the iron content of a liquid (FeO_L) for any assumed MgO content of the liquid (MgO_L) and melt fraction F, given FeO_o and MgO_o for any peridotite source composition. For melting on the solidus where $F \rightarrow 0$, FeO–MgO solutions to these equations are essentially identical to those derived from equation (18) for the olivine–liquid equilibrium for peridotite compositions KR-4003, MM3 and PHN1611. For olivine–liquid and harzburgite–liquid equilibria, solutions to equations (21), (22) and (23) at elevated melt fractions yield FeO–MgO–F systematics that are identical to those that have been independently calculated from mass balance solutions to the batch melting equation for all oxide components. However, solutions to equations (21)–(23) are applicable to all phase assemblages and at all melt fractions. These equations have therefore been applied to FeO–MgO–F systematics for phase assemblages ranging from the solidus to [L + Ol + Opx] in Figs 4b and 5a for Fe-rich fertile peridotite and depleted peridotite.

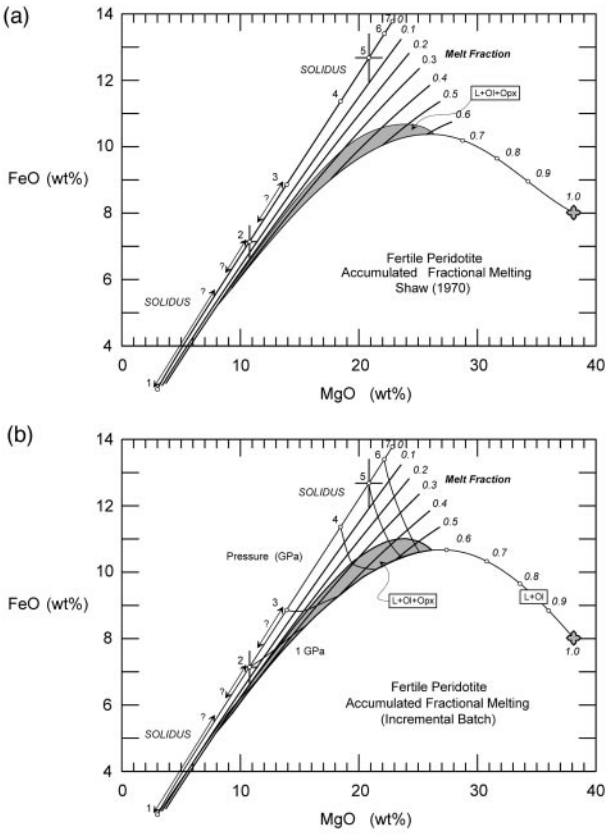

Fig. 6. (a) FeO and MgO contents of liquids formed by accumulated perfect fractional melting of fertile peridotite KR-4003, from solutions to Shaw's (1970) equation, (24), given in the text. (b) FeO and MgO contents of liquids formed by isobaric accumulated perfect fractional melting of fertile peridotite KR-4003, from solutions to the incremental batch melting equation for a continuously depleted residue. At the point of Opx exhaustion, olivine is the sole residuum phase (see text). It should be noted that FeO–MgO–F systematics are the same as in (a).

A forward model for FeO–MgO–F systematics specific to isobaric accumulated perfect fractional melting (APFM) of a fertile peridotite source (FeO ~8·0%)

Liquids formed by isobaric accumulated fractional melting were determined by first computing equilibrium liquid and residue compositions using equation (13) for equilibrium melting as discussed above. This provides a set of D and F values that were then used in Shaw's (1970) equation for accumulated fractional melting:

$$C_L = C_o[1 - (1 - F)^{1/D}] / F. \quad (24)$$

The computational procedure is discussed in more detail in Electronic Appendix 4 on the *Journal of Petrology* Web site at http://www.petrology.oupjournals.org. Results are shown in Fig. 6a.

An apparent paradox of Shaw's (1970) equations for fractional and accumulated fractional melting is that the MgO content of the residue becomes greater than the MgO content of olivine when olivine is the sole residue phase, a problem that is also discussed in Electronic Appendix 4. We therefore examine accumulated perfect fractional melting using the following incremental batch melting approach. We compute liquid compositions with 0·01 mass fractions of melting of the residue, the liquid is completely removed from its residue, the residue is melted again at successive 0·01 mass fractions, and each new melt is perfectly extracted and mixed with the previously formed melt. The process is repeated many times until the residue is completely melted, and each instantaneous melt is formed by equilibrium melting of an instantaneous residue whose composition is continuously changing owing to melt extraction. Each 0·01 mass fraction of melt extracted from the residue is called an 'instantaneous' drop of melt. This analysis is restricted to fertile peridotite KR-4003 for which we have pressure information. We consider first the case of isobaric melting at 1–6 GPa, and this is followed by consideration of polybaric melting situations.

The MgO content of the instantaneous liquid is computed from

$$C_{\mathrm{MgO,Lin}} = C_{\mathrm{MgO,Sin}}/[F_{\mathrm{S}}(1-D_{\mathrm{MgO,in}}) + D_{\mathrm{MgO,in}}] \quad (25)$$

where $C_{\mathrm{MgO,Lin}}$ is the weight percent MgO content of the instantaneous drop of liquid, $C_{\mathrm{MgO,Sin}}$ is the MgO content of the instantaneous solid residue, $D_{\mathrm{MgO,in}}$ is the weight percent partition coefficient of MgO between the residue and liquid, and $F_{\mathrm{S}} = 0{\cdot}01$, a constant mass fraction of melting of the residue S; it is worth noting that we could have chosen lower values for F_{S} but this has little effect on the computed liquid compositions. At each pressure, we parameterize $D_{\mathrm{MgO,in}}$ as a function of $C_{\mathrm{MgO,Sin}}$, and these are obtained from liquid compositions for isobaric equilibrium melting (Fig. 4a). For phase assemblages between the solidus and the onset of harzburgite melting, $D_{\mathrm{MgO,in}}$ is a nonlinear function of $C_{\mathrm{MgO,Sin}}$ at 1–3 GPa, but the function becomes linear at 4–6 GPa. For the harzburgite phase assemblage [L + Ol + Opx] we obtain $D_{\mathrm{MgO,in}}$ and $C_{\mathrm{MgO,Sin}}$ from solutions to equations (13) and (20), and these are modestly nonlinear. When olivine is the only residuum phase [L + Ol], it melts incongruently to a liquid on the forsterite–fayalite join where $K_{\mathrm{D}}^{\mathrm{Ol/L}}{}_{\mathrm{FeO/MgO}} = 0{\cdot}36$ (Fig. 2a). The situation for FeO is similar:

$$C_{\mathrm{FeO,Lin}} = C_{\mathrm{FeO,Sin}}/[F_{\mathrm{S}}(1-D_{\mathrm{FeO,in}}) + D_{\mathrm{FeO,in}}] \quad (26)$$

but D for FeO is obtained from

$$D_{\mathrm{FeO,in}} = 0{\cdot}036 + 0{\cdot}350D_{\mathrm{MgO,in}} - 0{\cdot}0094(D_{\mathrm{MgO,in}})^2 \quad (27)$$

by solutions to equations (13) and (20). We can obtain the exchange coefficient $K_{\mathrm{D}}^{\mathrm{S/L}}{}_{\mathrm{FeO/MgO}}$ by dividing $D_{\mathrm{FeO,in}}$ by $D_{\mathrm{MgO,in}}$, and this becomes equation (21).

The amount of liquid produced at the first increment of melting is 0·01, and this becomes progressively lower than 0·01 with each subsequent increment of melting because the mass of residue is progressively being reduced from 1·0 to zero. We keep track of the melt fraction of each increment with respect to the initial source mass, and call this F_{in}. Therefore, at the first increment of melting $F_{\mathrm{in}} = F_{\mathrm{S}}$, but during subsequent increments $F_{\mathrm{in}} < F_{\mathrm{S}}$. For the total melt fraction

$$F = \sum_{i=1}^{\mathcal{N}} F_{\mathrm{s}} \quad (28)$$

for $\mathcal{N}$ increments of melting. The average composition of the aggregate melt C_{L} is simply the compositions of the instantaneous melts (i.e. C_{Lin}) weighted according to the mass of each increment with respect to the initial source mass (i.e. F_{in}). For MgO and FeO this becomes

$$C_{\mathrm{L}} = (1/F)\sum_{i=1}^{\mathcal{N}} (C_{\mathrm{Lin}}F_{\mathrm{in}}). \quad (29)$$

For constant D, this incremental solution to the batch melting equation for perfect melt extraction yields results that are identical to those calculated using the equations of Shaw (1970). That is, the instantaneous batch liquid composition is identical to Shaw's (1970) perfect fractional melt composition, and the aggregated melt compositions in both cases are also the same.

Results for fractional melting of fertile peridotite with variable D are shown in Fig. 6a and b. Liquids formed by accumulated fractional melting have higher FeO contents than those for liquids that form by equilibrium melting (Fig. 4a) at any specific melt fraction, a conclusion reached previously by Langmuir *et al.* (1992). The most important observation is that identical FeO–MgO–F systematics are obtained for accumulated fractional melts calculated with Shaw's (1970) equation and incremental solutions to the batch melting equation. The utility of the incremental batch approach is that it can be easily applied to polybaric melting, as discussed below, and it can be modified to include imperfect melt extraction, a problem we will not consider further. However, a close examination of Fig. 6a and b reveals several minor but important differences. The incremental batch melting approach (Fig. 6b) provides pressure information whereas Shaw's (1970) equation does not. Additionally, there are minor differences in the compositions of aggregate liquids that form when olivine is the sole residue phase, an issue that is discussed further in Electronic Appendix 4.

Residue compositions of equilibrium and fractional melting are important for a complete mass balance analysis of peridotite melting, and bear on many problems of geological interest. Although a comprehensive discussion of residues is beyond the scope of this paper, there are several important aspects of this problem that require discussion. We consider only the *mg*-numbers of olivines in the residues. For the case of equilibrium melting of fertile peridotite, the *mg*-number of olivine increases from 89·5 to 95·9 from the solidus to the liquidus (Fig. 7a). For equilibrium melting of depleted peridotite, the *mg*-number of olivine increases from 90·2 to 96·2 from the solidus to the liquidus (Fig. 7a). The effect of perfect fractional melting is to produce residual olivines with *mg*-numbers that increase to 100 at the liquidus (Fig. 7b) for both depleted and fertile peridotite compositions. We consider now olivine phenocrysts with *mg*-numbers of 92·0 precipitated from an aggregate magma formed by accumulated perfect fractional melting of a fertile or depleted source. Olivines in the residue of the pooled liquid are in equilibrium with the last drop of perfect fractional melt, and these have *mg*-numbers of about 94·0 (Fig. 7b). A primary accumulated magma has a unique residue, but the accumulated liquid is not in equilibrium with that residue; only the final drop of liquid extracted is in equilibrium with the residue. This is the process treated by Gast (1968) and Shaw (1970) and specifies that the liquids that are integrated are

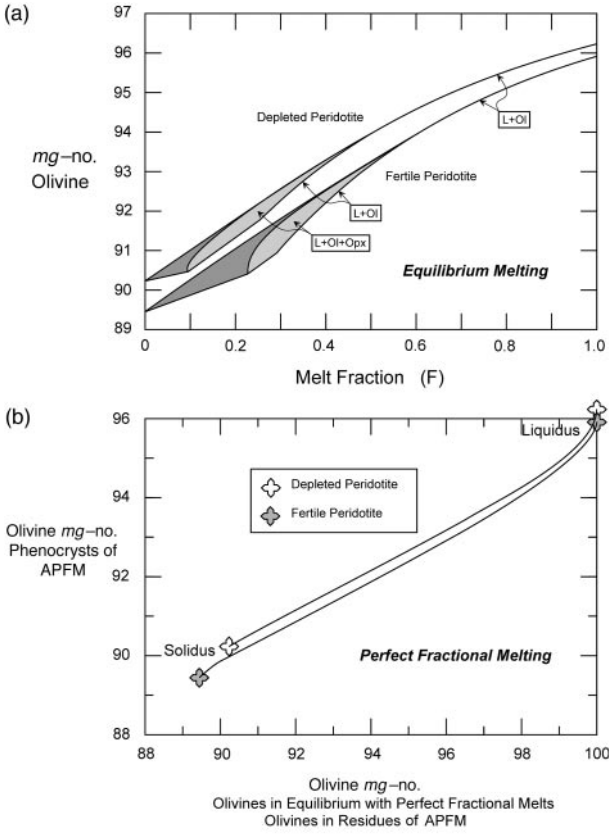

Fig. 7. (a) Olivine *mg*-number as a function of melt fraction for equilibrium melting of fertile peridotite KR-4003 and depleted peridotite. (b) Olivine *mg*-number in phenocrysts of primary magmas produced by accumulated perfect fractional melting (APFM) compared with *mg*-numbers of olivines in the residues and olivines that precipitate from perfect fractional melts. It should be noted that residues of fractional melts and accumulated perfect fractional melts are the same. *Mg*-numbers = 100 when $F = 1$.

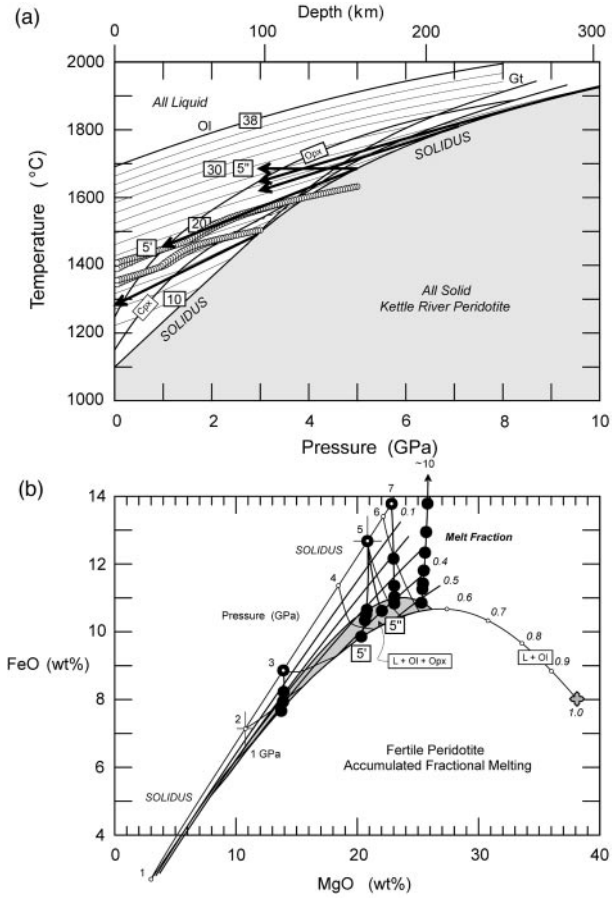

Fig. 8. (a) A temperature–pressure phase diagram for fertile peridotite KR-4003. Numbers in boxes are weight percent MgO contents of liquids (Electronic Appendix, Table A1). Anhydrous solidus for mantle peridotite is from Herzberg *et al.* (2000), and is almost identical to that offered by Hirschmann (2000) except that it is higher by about 30°C at 3–4 GPa. The difference between calculated temperatures and those in all experiments conducted by Walter (1998) averages 16°C at 3–7 GPa, but our preferred solidus is higher than Walter's by 50°C at 5 GPa. Adiabatic gradients indicated by small circles are from Asimow *et al.* (2001). Adiabatic gradients indicated by arrows are revised from Iwamori *et al.* (1995). Arrow indicated by 5″ is a hypothetical isothermal polybaric path initiated at 5 GPa; arrow indicated by 5′ is a more realistic polybaric path, modified from Iwamori *et al.* (1995; see text). It should be noted that most adiabatic gradients are approximately parallel to isopleths of MgO in equilibrium liquids. (b) Calculated FeO and MgO contents of accumulated fractional melts that are produced along the adiabatic gradients indicated by arrows in (a). Pressures of initial melting are 3, 5, 7 and 10 GPa. Solidus composition at 10 GPa is from Herzberg & Zhang (1996). Circles represent a 1 GPa drop in the pressure of final melting along each adiabatic gradient. Each decompression melting path exhibits a strong reduction in FeO at nearly constant MgO.

produced from a progressively depleting residue and are then added in aliquots to the final accumulation.

A forward model for FeO–MgO–F systematics specific to polybaric accumulated perfect fractional melting (APFM) of a fertile peridotite source (FeO ~8·0%)

An examination is now made of perfect polybaric accumulated fractional melting of fertile peridotite KR-4003. Before proceeding with the FeO and MgO characteristics of such melts, we consider the range of temperatures and pressures under which decompression melting can occur, and we do this with aid of the phase diagram for Kettle River peridotite KR-4003 shown in Fig. 8a. The anhydrous solidus for mantle peridotite is from Herzberg *et al.* (2000), which is almost identical to that offered by Hirschmann (2000) except that it is higher by about 30°C at 3–4 GPa. Temperatures for olivine-in and orthopyroxene-in were computed using the method of Beattie (1993) for liquid in equilibrium with olivine ± orthopyroxene at 1 atm, and extended to high pressures by a recalibration with experimental data sum-

marized above for K_D. Using 322 data points from 0·2 to 7·0 GPa and 1100 to 1950°C, we have obtained minimum residuals between observed and calculated temperatures with

$$T = T_{1\,atm} + 54P - 2P^2 \quad (30)$$

where T (°C) is the temperature of interest at pressure P (GPa), and $T_{1\,atm}$ (°C) is obtained from Beattie (1993) at 1 atm. Using equation (30) the difference between calculated and observed temperatures is ± 31°C at the 1σ level for pressures up to 7 GPa; this is only marginally higher than that obtained by Beattie (1993) for a much smaller dataset to 4 GPa. Temperatures for Cpx- and Gt-in were calculated for harzburgite-saturated liquids at the point of saturation in Cpx and Gt as defined by Fig. 1. The difference between calculated temperatures and those in all experiments conducted by Walter (1998) at 3–7 GPa on this same peridotite composition averages 16°C.

We examine the FeO and MgO contents of liquids that are formed along the five T–P paths shown in Fig. 8a, where melting initiates at 3, 5, 7 and 10 GPa. In one case the melting path is isothermal, and the other four approximate adiabatic gradients from Iwamori *et al.* (1995) but modified to remove 'bumps' that arose from strong T–P curvature to their solidus for spinel-lherzolite (Herzberg *et al.*, 2000). The other adiabatic T–P paths shown in Fig. 8a are from Asimow *et al.* (2001). Although we consider only linear paths in T–P space, the conclusions that follow are applicable to more realistic decompression melting paths. Fractional melt compositions were computed using equations for isobaric incremental batch melting, except that $D_{MgO,in}$ was parameterized as a polybaric function of $C_{MgO,Sin}$; values of $D_{MgO,in}$ and $C_{MgO,Sin}$ at each pressure along the polybaric path were parameterized from solutions to isobaric equilibrium melting (Fig. 4a). Instantaneous residue compositions vary continuously along each melting path owing to perfect melt extraction. Compositions of the accumulated melts were calculated from perfect fractional melts along each path between the solidus and the final melting pressure. Final melting pressures vary at 1 GPa increments below the initial melting pressure. Results are shown in Fig. 8b.

In most cases there is a substantial drop in the FeO content of liquids with decompression, but MgO varies by no more than 2% despite considerable differences in the melting paths (Fig. 8b). The reason why there is little change in MgO is because all T–P melting paths are approximately coincident with T–P isopleths of MgO in liquids defined by olivine saturation surfaces (Fig. 8a). Dissolution of 'wall-rock' olivine into ascending magmas should not be significant, and olivine–liquid equilibrium temperatures must closely reflect actual eruption temperatures. An important corollary is that the MgO content of a primary magma is similar to the MgO content of the initial melt on the solidus, and it reflects the pressure of initial melting.

There is also an important relationship between aggregate polybaric and isobaric melt compositions. Let us consider the case of decompression melting starting at 5 GPa and terminating at about 1·5 GPa along the path designated at 5′ in Fig. 7a and b. The aggregate melt composition has 20·5% MgO and 10·1% FeO and is formed at a melt fraction of 0·40. This same melt composition is formed isobarically at 4 GPa, also at an average melt fraction of 0·40 (Fig. 8b). The aggregate magma formed polybarically therefore records in its geochemistry an average pressure of 4 GPa, as defined by isobaric 4 GPa FeO–MgO–F relations.

For melting regimes in oceanic ridges and mantle plumes, there will be an infinite number of streamlines, with horizontal and vertical components, along which fractional melts are formed and in local equilibrium with their residues. The melting regime may then be visualized as a spider's web of streamlines, and the primary aggregate magma is an integrated product of all fractional melts that collect in the melting regime. Any true forward melting model must therefore compute the compositions of all fractional melts along all streamlines, and then perform the integration within the melting regime. The complexity of this procedure is immediately apparent. The importance of isobaric FeO–MgO–F systematics is that they provide a simple means of constraining the composition of a primary aggregate melt for any melting regime, regardless of the polybaric streamline complexity. This is explored in the subsequent discussion.

Forward models for FeO–MgO–F systematics specific to accumulated perfect fractional melting (APFM) of depleted and iron-rich peridotite source

Liquids in equilibrium with olivine [L + Ol] and harzburgite residues [L + Ol + Opx] were discussed above (Fig. 5b). The bulk distribution coefficients D for FeO and MgO were used together with F and Shaw's (1970) equation, (24), to calculate liquids formed by accumulated perfect fractional melting. Results are illustrated below in the discussions on Gorgona and Hawaiian magmatism. We cannot provide pressure information for the aggregate liquids because it is not known for equilibrium melting.

INVERSE MODELS

We restrict our inverse models to well-documented high-MgO aphyric and olivine-phyric lavas that are related to each other in space and time by fractional crystallization of olivine. We assume that olivine was the sole

fractionating phase that relates all lavas to each other and all lavas to the primary magma from the melting regime. The inversion method consists of selecting a representative lava composition into which olivine is incrementally added or from which olivine is incrementally subtracted. The composition of olivine in local equilibrium with the liquid is computed by the method discussed above, where $K_D^{Ol/L}{}_{FeO/MgO}$ is adjusted for changes in liquid composition, and each increment represents 1 wt % addition or subtraction of olivine. These inverse calculations produce a loci of compositions that can be compared with the compositions of liquids in the various forward models discussed above. A computational algorithm is provided in Electronic Appendix 5 on the *Journal of Petrology* Web site at http://www.petrology.oupjournals.org so that the reader can replicate our calculations.

Several workers, in attempts to compute mid-ocean ridge basalt (MORB) and hotspot primary magmas, have assumed that all Fe in published lava analyses was FeO (i.e. FeO_T; Langmuir *et al.*, 1992), whereas others have attempted to consider only the true amount of FeO in the lava that is exchangeable with olivine (Albarède, 1992; Nisbet *et al.*, 1993; Larsen & Pedersen, 2000). We adopt the latter approach because the amount of Fe_2O_3 can be large, with $Fe^{3+}/\Sigma Fe$ ranging from about 0·07 to 0·15 in most MORB and komatiite occurrences reviewed below. Only when both FeO and Fe_2O_3 are evaluated in a lava suite of interest can we make a comparison with our forward models where iron has been calculated strictly as FeO from the exchange coefficient $K_D^{Ol/L}{}_{FeO/MgO}$. Failure to do so can result in substantial errors. For example, in the case where MgO = 20·0%, FeO_T = 10·0% and $Fe^{3+}/\Sigma Fe$ = 0·10, it can be determined that Fe_2O_3 = 1·11% and FeO = 9·0%. Inspection of Fig. 4 reveals that use of 10% FeO_T instead of 9·0% FeO would yield a pressure for an equilibrium primary magma that is about 2 GPa too high.

For Kilauea and Baffin Island lavas we use FeO and Fe_2O_3 that have been directly measured by wet chemistry ($Fe^{3+}/\Sigma Fe$ = 0·1; Wright *et al.*, 1975; Robillard *et al.*, 1992). In all cases we treat lavas that move from the melting regime to the surface as a system that is closed to oxygen, and assume no change in $Fe^{3+}/\Sigma Fe$ for both primary and derivative lavas. A small but additional source of uncertainty is that we compare lavas for which both FeO and Fe_2O_3 have been constrained with forward models that contain no Fe_2O_3, as for fertile peridotite KR-4003 and its Fe-rich analogue. Although it is possible to include Fe_2O_3 in the forward model computations for olivine- and harzburgite-saturated liquids, as has been done for the depleted peridotite composition, the partition coefficients are not well constrained for assemblages containing garnet and clinopyroxene. Primary komatiite magmas are expected to contain 1–2% Fe_2O_3, and this will result in a modest dilution of all oxide elements in our computed forward models. For example, a primary magma with 10% FeO we calculate in a forward model would actually contain 9·8% FeO if it also had 2% Fe_2O_3 (10% FeO × 98/100). Our forward and inverse models should therefore be useful in situations where the amount of $Fe^{3+}/\Sigma Fe > 0{\cdot}1$.

In cases where FeO and Fe_2O_3 have not been directly measured in the lavas (i.e. West Greenland and Gorgona), they have been computed from FeO_{total} using the method of Kress & Carmichael (1991) and estimates of oxygen fugacity (Canil, 1999; Larsen & Pedersen, 2000). Oxygen fugacities are compared with those for the following buffers: nickel–nickel oxide (NNO) from O'Neill & Pownceby (1993), fayalite–quartz–magnetite (FQM) from O'Neill (1987), and iron–wüstite (IW) from O'Neill & Pownceby (1993). For example, Christie *et al.* (1986) determined $Fe^{3+}/\Sigma Fe = 0{\cdot}07 \pm 0{\cdot}03$ for 78 MORB glasses. An fO_2 = 2·5 log units more reducing than the NNO buffer (i.e. NNO − 2·5) would yield $Fe^{3+}/\Sigma Fe$ = 0·07 for MORB using the method of Kress & Carmichael (1991), although different parameters in Kilinc *et al.* (1983) provide the same $Fe^{3+}/\Sigma Fe$ with NNO = −2·3 (Christie *et al.*, 1986). Data of Wright *et al.* (1975) on eruptions between 1968 and 1971 exhibit $Fe^{3+}/\Sigma Fe$ = 0·10, only slightly more oxidizing than MORB ($Fe^{3+}/\Sigma Fe$ = 0·07; Christie *et al.*, 1986). A ratio of $Fe^{3+}/\Sigma Fe$ = 0·10 is characteristic of an fO_2 = 1·3 log units more reducing than the NNO buffer (i.e. NNO − 1·3; O'Neill & Pownceby, 1993).

Another minor difficulty with the inverse method is that addition and subtraction of olivine will yield a primary magma with $Fe^{3+}/\Sigma Fe$ that differs somewhat from the selected lava composition because olivine accepts no Fe_2O_3. For example, the primary magma we calculate for Kilauea by adding olivine to sample DAS69-5-1 (Wright *et al.*, 1975) contains 1·01–1·03% Fe_2O_3, whereas it should contain 1·18–1·19% Fe_2O_3 at NNO − 1·3 (Table 4). We have made no corrections for this effect because the error is small and overwhelmed by uncertainties in K_D. Another difficulty is that we have completely ignored the effects of chromite precipitation. Our estimates for Cr_2O_3 in primary magmas are therefore unreliable.

GORGONA KOMATIITES: AN EXAMPLE OF A HYBRID FORWARD–INVERSE MODEL

Detailed geochemical descriptions of Cretaceous picrites and komatiites from Gorgona Island have been provided by Echeverria (1980), Aitken & Echeverria (1984), Echeverria & Aitken (1986), Kerr *et al.* (1996), Arndt *et al.*

Table 4: Calculated Gorgona primary magma compositions (wt %)

	1E	1F	2E	2F	3E	3F
Source type:	Fertile	Fertile	Depleted	Depleted	Fertile	Fertile
Source wt % FeO:	8·0	8·0	8·0	8·0	9·0	9·0
Melting mechanism:	EQ	APFM	EQ	APFM	EQ	APFM
SiO_2	45·8	46·1	45·9	46·1	46·3	46·6
TiO_2	0·53	0·56	0·54	0·56	0·58	0·61
Al_2O_3	10·9	11·7	11·3	11·7	12·1	12·8
Cr_2O_3	0·15	0·16	0·15	0·16	0·16	0·17
Fe_2O_3	1·10	1·18	1·14	1·18	1·22	1·30
FeO	10·0	10·1	10·1	10·1	10·2	10·2
MnO	0·17	0·18	0·18	0·18	0·18	0·18
MgO	20·9	18·8	20·0	18·8	17·9	16·0
CaO	9·3	10·0	9·6	10·0	10·3	10·9
Na_2O	0·97	1·04	1·00	1·04	1·07	1·14
K_2O	0·03	0·03	0·03	0·03	0·03	0·03
NiO	0·141	0·112	0·128	0·112	0·100	0·076
Olivine *mg*-no.	91·5(0·4)	90·6(0·5)	91·1(0·4)	90·6(0·5)	90·2(0·5)	89·3(0·5)
F (melt fraction)	0·26	0·28	0·12	0·11	0·27	0·26
P (GPa)	4·0	3·8	3·8	n.d.	3·0	n.d.
T @ 4 GPa (°C)	1641	1606	1626	1606	1590	1555
T @ 1 atm (°C)	1457	1422	1442	1422	1406	1371

Gorgona: olivine addition to and subtraction from sample 149 (Aitken & Echeverria, 1984). EQ, equilibrium melting; APFM, accumulated perfect fractional melting. Fertile source with 8·0% FeO is Kettle River peridotite (Table 1). Depleted source with 8·0% FeO is abyssal peridotite (Table 1). Fertile source with 9·0% FeO is Fe peridotite (Table 1). Olivine *mg*-number in parentheses is 1σ uncertainty arising from $K_D^{Ol/L}{}_{FeO/MgO}$. *P* is pressure for equilibrium melting and average pressure for accumulated fractional melting; *T* @ 4·0 GPa and *T* @ 1 atm are temperature of liquid in equilibrium with olivine at 4·0 GPa and 1 atm, respectively (see text); n.d., not determined.

(1997) and Révillon *et al.* (2000). The terms 'picrite' and 'komatiite' have been used to describe hyaloclastic volcanic rocks without spinifex textures and lava flows with spinifex textures, respectively. We will retain these terms.

Komatiite lavas are shown in Fig. 9a and b for an fO_2 at NNO − 1·3. This is similar to that for Kilauea, and to fO_2 estimated by Canil (1999; NNO − 1·5 ± 1·5) for Gorgona. Olivine fractionation dominates major element geochemistry, and we select a representative composition from Aitken & Echeverria (1984; Table 4) for which olivine is added and subtracted. This is the inverse model component that defines the locus of possible primary magma compositions shown in Fig. 9a and b. The forward model component is shown also in Fig. 9a and b, that being for accumulated perfect fractional melting of an assumed fertile peridotite source, composition KR-4003 in Table 1. We can uniquely determine the primary magma composition by interfacing the projection in Fig. 9a with the FeO–MgO diagram in Fig. 9b by searching for a composition that provides a unique melt fraction *F*. That melt fraction *F* is 0·28, yielding 18·8% MgO and 10·0% FeO and an average pressure of 3·8 GPa (Fig. 9b; Table 4). For Gorgona and all other cases considered in this paper, the melt fraction provides the link between inverse and forward models.

An average pressure of 3·8 GPa is obtained for the primary magma formed by accumulated perfect fractional melting of a fertile peridotite source. This pressure probably has little significance because it is specific to a fertile peridotite source, and there exist substantial uncertainties stemming from experimental calibrations. Also, as discussed above, no pressure information is obtainable for forward models involving depleted and Fe-rich peridotite.

The primary magma composition would precipitate olivine phenocrysts having an *mg*-number of 90·6 (±0·5; Table 4), and fractional crystallization would produce derivative liquids that would crystallize olivines with lower *mg*-numbers. Our calculated olivines are in good

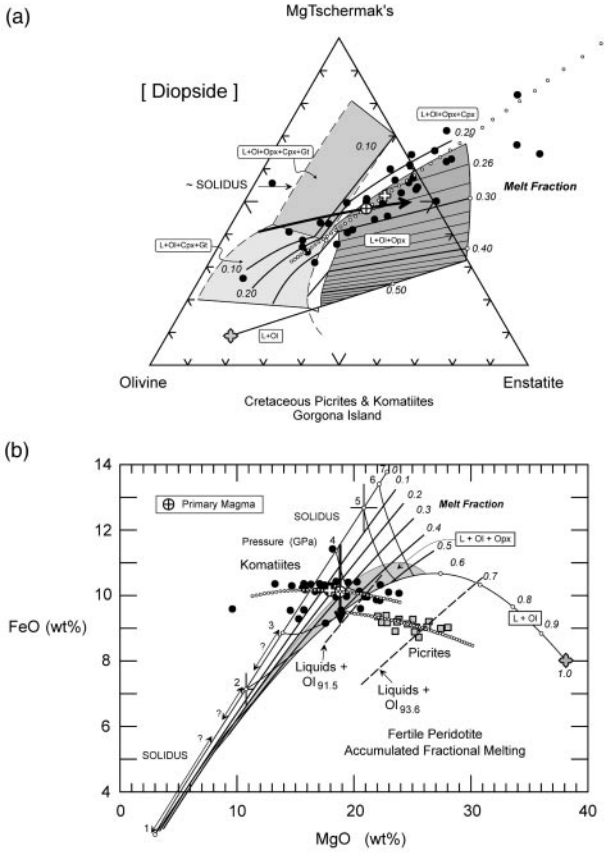

Fig. 9. (a) A projection of liquid compositions in equilibrium with fertile mantle peridotite, from Fig. 1b, and Gorgona komatiites superposed. Filled circles, Gorgona komatiites; open cross, komatiite sample 149 (Aitken & Echeverria, 1984) for which olivine was added to and subtracted from (small circles); cross-in-circle, primary magma for accumulated fractional melting; arrow, approximate locus of compositions produced along an adiabatic decompression melting path. (b) FeO–MgO for accumulated fractional melting of fertile peridotite, from Fig. 6b, and Gorgona komatiites and picrites. Symbols as for (a).

agreement with *mg*-numbers of about 90–91 that are commonly observed for skeletal olivines in spinifex-textured komatiites (Révillon *et al.*, 2000). However, rare olivines with *mg*-numbers of about 91·5 have also been reported (Aitken & Echeverria, 1984; Révillon *et al.*, 2000), and these can be in equilibrium with the locus of possible FeO and MgO contents in liquids shown in Fig. 9b. One way of explaining $Ol_{91·5}$ is to have more MgO in the primary magma by adding more olivine to the derivative magma in the inverse model. This approach yields a primary magma with 21% MgO rather than 18·8% in our model, but with contradictory phase equilibrium properties (i.e. L + Ol in FeO–MgO space but L + Ol + Opx + Gt in projection). Another way of explaining $Ol_{91·5}$ is by reducing the FeO content of the magma. Indeed, an aggregate magma that precipitates $Ol_{90·6}$ can be a mixture of perfect fractional melts in equilibrium with $Ol_{89·4}$ at the solidus to $Ol_{91·5}$ at the maximum extent of melting (Fig. 7b). This range of olivine compositions could form during decompression from an initial melting pressure of about 4·2 GPa (Fig. 9b), and $Ol_{91·5}$ could have precipitated from advanced fractional melts with lower FeO contents than the accumulated fractional melts (Fig. 9b). The implication is that the mixing of fractional melts within the melting regime was not a perfect process. This explanation can account for the outliers in FeO contents seen for komatiites (Fig. 9b), and it will be raised again in the discussion on Gorgona picrites.

It is reasonable to question the appropriateness of using an assumed fertile peridotite composition in the forward model because trace elements and isotopes for Gorgona komatiites indicate a depleted MORB-like source (Echeverria, 1980; Kerr *et al.*, 1996; Arndt *et al.*, 1997). We therefore use the depleted peridotite source in Table 1 in another forward model of accumulated fractional melting, and results are shown in Fig. 10a and b. Again, we determine the primary magma composition by interfacing the projection in Fig. 10a with the FeO–MgO diagram in Fig. 10b by searching for a composition that provides a unique melt fraction F in both cases. The melt fraction is 0·11, yielding a primary magma with 18·8% MgO and 10·0% FeO, which is identical to the primary magma composition for the fertile peridotite source. We consider six possible primary magma compositions from solutions for equilibrium and accumulated fractional melting for three different peridotite source compositions. Results are listed in Table 4. For fertile and depleted source compositions, the MgO contents are restricted to 18·8–20·9%, in agreement with other estimates for MgO (Nisbet *et al.*, 1993; Kerr *et al.*, 1996; Révillon *et al.*, 2000). However, melt fractions vary considerably, from 0·11 for the depleted source to 0·28 for the fertile source.

All primary magmas plot within the harzburgite stability field [L + Ol + Opx], near the melt fraction defined by Cpx-out in both projection and in FeO–MgO plots (Figs 9 and 10). Harzburgite is therefore the residue for these primary magmas. All primary magmas formed by accumulated fractional melting must display internal consistency in residuum mineralogy when viewed in projection and FeO–MgO plots.

Picrites at Gorgona are generally lower in FeO and higher in MgO than komatiites, and they have maximum *mg*-numbers in the 93·3–93·6 range (Echeverria & Aitken, 1986; Révillon *et al.*, 2000). It can be seen in Figs 9b and 10b that the komatiites could not have formed from the picrites by fractional crystallization of olivine, a conclusion reached also by Arndt *et al.* (1997). It can also be seen that the picrites could not have formed from the primary komatiite by advanced accumulated fractional melting; higher melt fractions would yield a primary

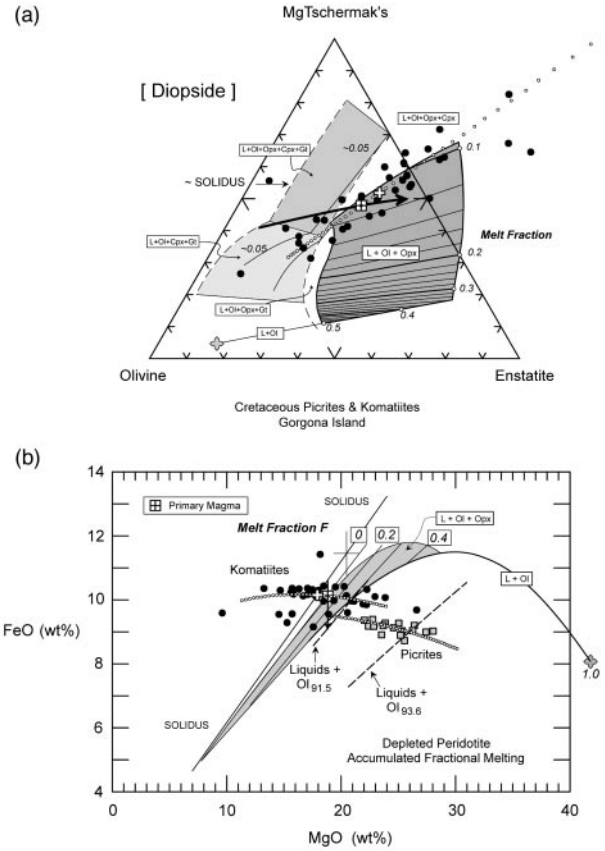

Fig. 10. (a) A projection of liquid compositions in equilibrium with depleted mantle peridotite, from Fig. 1b, and Gorgona komatiites superposed. Cross-in-square, primary magma for accumulated fractional melting. All other symbols as for Fig. 9a. (b) FeO–MgO for accumulated fractional melting of depleted peridotite and Gorgona komatiites and picrites. Cross-in-square, primary magma. All other symbols as for Fig. 9b.

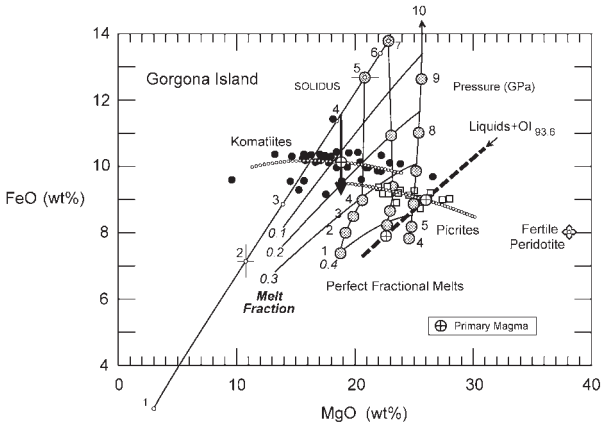

Fig. 11. FeO–MgO for perfect fractional melts of fertile peridotite compared with Gorgona komatiites and picrites. FeO and MgO contents of perfect fractional melts are calculated along the polybaric and polythermal adiabatic gradients indicated by arrows in Fig. 8a. Circles represent a 1 GPa drop in the pressure of final melting along each adiabatic gradient. It should be noted that possible picrite primary magmas can plot anywhere along the locus of liquid compositions in equilibrium with olivine having an *mg*-number of 93·6; these range from 22 to 26% MgO. Arrow indicates approximate locus of compositions produced along an adiabatic decompression melting path appropriate for the komatiites, from Fig. 9b. Melt fractions refer to total melting of initial source mass.

picrite magma with slightly higher FeO, the opposite of what is observed (Fig. 9b). Indeed, any picrite that precipitates $Ol_{93\cdot6}$ is too low in FeO to be an accumulated fractional melt of either fertile or depleted mantle peridotite.

Arndt *et al.* (1997) interpreted the rare earth element geochemistry of Gorgona lavas by a dynamic fractional melting process wherein a hot plume interior loses its melt and leaves behind a refractory source that is subsequently melted to form the picrites. This open-system melting process can be modelled with fractional melts that do not mix, using equations (25) and (26). Shown in Fig. 11 are perfect fractional melts formed polybarically along three adiabatic melting paths in Fig. 8a. The effect of advanced partial melting during decompression is to form perfect fractional melts with lower FeO contents without much change in MgO (Fig. 11). The mixing of perfect fractional melts with a wide range of FeO yields accumulated fractional melts with the average FeO contents shown in Fig. 8b. There exists a locus of possible FeO and MgO contents of perfect fractional melts that will be in equilibrium with olivine having an *mg*-number of 93·6 (Fig. 11). Of these, a primary picrite magma with about 26% MgO is possible and consistent with that estimated by Révillon *et al.* (2000). For an assumed fertile peridotite source, this primary magma would have required an initial melting pressure of about 10 GPa, a final melting pressure of about 6 GPa, and would have formed after 0·4 mass fractions of total melting of the initial source mass (Fig. 11). Another solution has initial melting at 7 GPa and final melting at 2·5 GPa where fractional melts will be in equilibrium with $Ol_{93\cdot6}$; in this scenario, the Gorgona picrites are mixtures biased with advanced fractional melts having a wide range in FeO but with about 23% MgO (Fig. 11). The range of permissible MgO contents is about 23–26%, demonstrating that olivine with an *mg*-number of 93·6 provides a limited constraint on primary magma composition. It is also not possible to rigorously constrain initial melting pressure for the picrites. However, it must have been higher than the 4·2 GPa that is required to explain the komatiites (Fig. 11). An initial melting pressure of 5 GPa is even too low as it could not yield perfect fractional melts with FeO contents low enough to yield $Ol_{93\cdot6}$. The picrites appear to have formed in the hottest and deepest part of the Gorgona plume axis, in agreement with conclusions drawn by Arndt *et al.* (1997).

Our calculations provide strong support for the interpretation that the Gorgona picrites formed by the dynamic fractional melting model proposed by Arndt *et al.* (1997). In this model, the picrites formed from the hot plume axis after the removal of earlier and lower-degree melts. Arndt *et al.* (1997) noted that these earliest formed melts may not have reached the surface because they have not been recognized on Gorgona or elsewhere, and that they may have been removed to another part of the plume. We concur that the picrites formed as fractional melts that did not mix with other fractional melts in the melting regime, and the komatiites formed as reasonably well-mixed aggregate fractional melts. Therefore, there must have been important restrictions to magma mixing in the Gorgona plume.

HAWAII (KILAUEA)

Recent estimates place the MgO content at 13–19% for Hawaiian primary magmas (Albarède, 1992; Eggins, 1992*a*; Hirschmann & Ghiorso, 1994; Baker *et al.*, 1996; Hauri, 1996; Norman & Garcia, 1999), and picrite glasses with 15% MgO have been directly observed (Clague *et al.*, 1991). We restrict our new analysis to an evaluation of the primary magma for historical eruptions on Kilauea, and use data reported by Murata & Richter (1966), Wright & Fiske (1971), Wright (1972, 1973), Wright *et al.* (1975), Clague *et al.* (1991) and Norman & Garcia (1999). Inverse modelling was performed on sample DAS69-5-1 from Wright *et al.* (1975), which contains 12·2% MgO. Solutions for the Kilauea primary magma composition are given in Table 5 for three assumed source compositions, and we offer in Electronic Appendix 6 on the *Journal of Petrology* Web site at http://www.petrology.oupjournals.org a detailed model for a fertile peridotite source. Primary Kilauea magmas contain 16·8–24·4% MgO (Table 5), but the upper end is for equilibrium melting, which is unlikely. Olivines that would crystallize from the remaining more likely primary magmas have *mg*-numbers in the 89·4–91·4 range (Table 5). These are in good agreement with maximum *mg*-numbers of 90·7 and 91·3 observed for olivines in Kilauea and Mauna Loa lavas, respectively (Norman & Garcia, 1999). Albarède (1992) estimated that olivines with similar *mg*-numbers precipitated from a primary magma containing 19·2% MgO, in good agreement with our estimates. We note that CaO contents of olivine phenocrysts are high (i.e. 0·20%; Norman & Garcia, 1999), which is consistent with an origin by precipitation from magmas (Table A1, Electronic Appendix 3) and inconsistent with an origin as accidental fragments of the mantle (e.g. Thompson & Gibson, 2000).

The major difference between models is in the melt fractions. Primary magmas with 16·8–21·3% MgO can be produced by 0·14–0·31 mass fractions of total melting, demonstrating the sensitivity of F to the composition of the source. A melt fraction of 0·15 has been independently estimated from uranium series disequilibria (Sims *et al.*, 1999), and depleted mantle has been identified as one of several isotopic components in the source (Feigenson, 1984).

It has been suggested that the Hawaiian source is lithologically heterogeneous, with eclogite or garnet pyroxenite veins within a peridotite host (Hauri, 1996; Lassiter & Hauri, 1998). This is at variance with conclusions drawn from combined hafnium–neodymium–thorium isotope systematics (Stracke *et al.*, 1999) and Na/Ti systematics (Putirka, 1999). It is also in contrast to our models that yield primary magma from a peridotite source. We do not dismiss the potential importance of subducted crust. Indeed, we discuss in Electronic Appendix 6 that the Kilauea source may have 1–4% by mass of subducted pelagic sediment. The essential question is whether subducted crust identified geochemically occurs also as a distinct lithological entity in the form of eclogite veins, a discussion that is raised in Electronic Appendix 6. If indeed the Hawaiian source region is a lithological mixture of peridotite and eclogite, then our primary magma compositions will be in error. However, we invite the proponents of lithological heterogeneity to offer a model that predicts the precipitation of olivines with *mg*-numbers of about 91.

TERTIARY PICRITES AND KOMATIITES FROM THE ICELANDIC PLUME

There are now many descriptions of Tertiary picrites and komatiites from Baffin Island and West Greenland (Drever, 1956; Drever & Johnston, 1957; Clarke, 1970; Clarke & Pedersen, 1976; Francis, 1985; Pedersen, 1985; Gill *et al.*, 1992; Larsen *et al.*, 1992; Robillard *et al.*, 1992; Holm *et al.*, 1993; Saunders *et al.*, 1997; Larsen & Pedersen, 2000; Scarrow *et al.*, 2000). Of these, inverse modelling was performed on sample 10014 from Baffin Island, an olivine-phyric lava with 11·85% MgO (Robillard *et al.*, 1992), and sample 113325 from Disko Island in West Greenland, a lava with 10·0% MgO (Holm *et al.*,1993). Baffin Island lavas contain $Fe^{3+}/\Sigma Fe = 0{\cdot}1$, based on wet chemistry (Robillard *et al.*, 1992), indicating an fO_2 similar to that for Kilauea (i.e. NNO − 1·3). However, Larsen & Pedersen (2000) inferred an fO_2 similar to NNO for West Greenland lavas, based on coexisting glass–chromite compositions.

Solutions for primary magma compositions are listed in Tables 6 and 7 for various assumed peridotite source compositions, and we offer in Electronic Appendix 7 on

Table 5: Calculated Kilauea primary magma compositions (wt %)

	1E	1F	2E	2F	3E	3F
Source type:	Fertile	Fertile	Depleted	Depleted	Fertile	Fertile
Source wt % FeO:	8·0	8·0	8·0	8·0	9·0	9·0
Melting mechanism:	EQ	APFM	EQ	APFM	EQ	APFM
SiO_2	46·4	47·2	47·0	47·3	47·4	48·0
TiO_2	1·60	1·85	1·78	1·87	1·9	2·05
Al_2O_3	8·1	9·4	9·1	9·5	9·7	10·5
Cr_2O_3	n.d.	n.d.	n.d.	n.d.	n.d.	n.d.
Fe_2O_3	0·91	1·06	1·02	1·07	1·09	1·18
FeO	10·1	10·4	10·3	10·4	10·4	10·5
MnO	0·16	0·17	0·17	0·17	0·17	0·18
MgO	24·4	20·2	21·3	19·9	19·3	16·8
CaO	6·7	7·8	7·5	7·9	8·0	8·6
Na_2O	1·38	1·60	1·54	1·61	1·65	1·78
K_2O	0·29	0·34	0·32	0·34	0·35	0·37
NiO	n.d.	n.d.	n.d.	n.d.	n.d.	n.d.
Olivine *mg*-no.	92·5(0·4)	90·9(0·5)	91·4(0·4)	90·8(0·5)	90·5(0·5)	89·4(0·5)
F (melt fraction)	0·38	0·31	0·14	0·14	0·30	0·28
P (GPa)	4·8	4·1	3·3	n.d.	2·5	n.d.
T @ 4 GPa (°C)	1697	1633	1651	1628	1618	1576
T @ 1 atm (°C)	1513	1449	1467	1444	1434	1392

Kilauea: olivine addition to sample DAS69-5-1 (Wright *et al.*, 1975). Abbreviations and explanation as for Table 4.

the *Journal of Petrology* Web site at http://www.petrology.oupjournals.org a detailed description for a depleted source. A depleted source is consistent with Sr and light rare earth element depletions for Baffin Island and Disko Island lavas (Robillard *et al.*, 1992; Holm *et al.*, 1993). Primary magmas from depleted and fertile peridotite sources (i.e. with 8·0% FeO) contain 17–20% MgO, in excellent agreement with previous estimates (Francis, 1985; Pedersen, 1985; Holm *et al.*, 1993; Larsen & Pedersen, 2000). The Fe-rich source composition yields primary magmas with MgO as low as 14% (Table 7).

Baffin Island lavas contained zoned olivine xenocrysts with core–rim *mg*-numbers of 93–89, although the maximum *mg*-number of 91·9 seems more common, and Francis (1985) concluded that they must have precipitated from liquids with more than 18% MgO. The interpretations of Francis (1985) are in good agreement with our forward model of a depleted source (Baffin 2F; Table 6), wherein we obtain a primary magma with 17·9% MgO in equilibrium with olivine having an *mg*-number of 90·6. Olivines that would crystallize from our estimated West Greenland primary magmas also have *mg*-numbers of around 90·5 (Table 7). Olivines with these compositions are observed in lavas from the Vaigat Formation, but rare olivines with *mg*-numbers as high as 93·0 also occur (Larsen & Pedersen, 2000), similar to those from Baffin Island (Francis, 1985). We discuss in Electronic Appendix 7 that $Ol_{93·0}$ could not have precipitated from any reasonable accumulated fractional melt. However, these high *mg*-number olivines are very similar to those for picrites from Gorgona. In our discussion above, we suggested that the picrites formed as fractional melts from the refractory Gorgona plume core, and a parallel explanation may hold true for the Icelandic plume. The difference, however, is that picritic melts with low FeO contents are not observed in the Icelandic plume lavas. We suggest that olivines with *mg*-numbers of 93·0 in Icelandic plume lavas may be wall-rock xenocrysts from the refractory plume core, and that the fractional melts that they were in equilibrium with may have been thoroughly mixed in the formation of the aggregate primary magma. Alternatively, they may be phenocrysts of perfect fractional melts that exited the melting regime and mixed with other melts during eruption. Without direct samples of these fractional melts, the MgO content cannot be constrained.

Ni partitioning experiments have been used to infer that primary magmas could not have MgO contents

Table 6: Calculated Baffin Island primary magma compositions (wt %)

	1E	1F	2E	2F	3E	3F
Source type:	Fertile	Fertile	Depleted	Depleted	Fertile	Fertile
Source wt % FeO:	8·0	8·0	8·0	8·0	9·0	9·0
Melting mechanism:	EQ	APFM	EQ	APFM	EQ	APFM
SiO_2	46·1	46·5	46·3	46·5	46·8	47·2
TiO_2	0·92	0·99	0·96	0·99	1·04	1·10
Al_2O_3	11·2	12·1	11·7	12·1	12·7	13·5
Cr_2O_3	0·09	0·09	0·09	0·09	0·09	0·10
Fe_2O_3	0·91	0·99	0·96	0·99	1·04	1·10
FeO	9·6	9·7	9·7	9·7	9·7	9·69
MnO	0·17	0·17	0·17	0·17	0·18	0·18
MgO	20·3	17·9	18·8	17·9	16·3	14·4
CaO	9·4	10·1	9·8	10·1	10·6	11·2
Na_2O	1·20	1·30	1·27	1·30	1·37	1·46
K_2O	0·04	0·04	0·04	0·04	0·04	0·05
NiO	0·147	0·110	0·124	0·110	0·088	0·064
Olivine *mg*-no.	91·6(0·4)	90·6(0·5)	91·0(0·5)	90·6(0·5)	89·9(0·5)	88·8(0·6)
F (melt fraction)	0·28	0·26	0·11	0·10	0·23	0·18
P (GPa)	3·6	3·5	3·1	n.d.	2·2	n.d.
T @ 4·0 GPa (°C)	1629	1588	1604	1588	1559	1521
T @ 1 atm (°C)	1445	1404	1420	1404	1375	1337

Baffin Island: olivine addition to sample 10014 (Robillard *et al.*, 1992). Abbreviations and explanation as for Table 4.

much greater than 13% because they would yield olivine-fractionated derivative liquids with Ni contents that are lower than those observed in lavas (Hart & Davis, 1978; Yaxley, 2000). We would not ordinarily add to the discussion that has followed (Clarke & O'Hara, 1979; Elthon & Ridley, 1979; Francis, 1985; Larsen & Pedersen, 2000), except that the Ni problem has been raised again for West Greenland volcanics (Yaxley, 2000). Contents of NiO and MgO were computed by incremental addition of olivine to lava 113325 (Holm *et al.*, 1993) using MgO-dependent partition coefficients for NiO between olivine and liquid (Beattie *et al.*, 1991; Table 2). Results shown in Fig. 12 demonstrate that a model primary magma with 17·2% MgO and 0·083% NiO yields calculated olivine phenocrysts, derivative liquids and olivine cumulates that are in good agreement with those that are observed in lava flows.

MID-OCEAN RIDGE BASALTS

It is useful to compare primary magmas from plume associations with those from mid-ocean ridges. The only occurrences of olivine-phyric MORB that we are aware of are those from the Reykjanes Peninsula on Iceland (Jakobsson *et al.*, 1978) and those from the Siqueiros transform fault that offsets the East Pacific Rise (Perfit *et al.*, 1996). We restrict this analysis to the Siqueiros MORB because the substantial variability of FeO reported by Jakobsson *et al.* (1978) on Reykjanes MORB compromises primary magma solutions. The record of olivine as a sole liquidus phase has been erased in all other MORB by gabbro and troctolite crystallization in crustal magma chambers (O'Hara, 1968*b*). Procedures are available for backtracking these effects (Langmuir *et al.*, 1992), but they are subject to some uncertainty (O'Hara & Herzberg, 2002).

Siqueiros MORB reported by Perfit *et al.* (1996) are fresh picritic basaltic lavas characterized by high-MgO glasses and 5–20 modal % olivine phenocrysts. Magmas that were primary to the MORB glasses were evaluated by incrementally adding olivine to MORB sample ALV2384-007B. This particular sample is a glass with the highest *mg*-number, and lowest Na_2O and TiO_2. Christie *et al.* (1986) determined $Fe^{3+}/\Sigma Fe = 0{\cdot}07 \pm 0{\cdot}03$ for 78 MORB glasses, and this ratio has been used to calculate FeO and Fe_2O_3 for the Siqueiros database (Perfit *et al.*, 1996).

Solutions for the primary magma composition are given in Table 8 and discussed in detail in Electronic Appendix

Table 7: Calculated West Greenland primary magma compositions (wt %)

	1E	1F	2E	2F	3E	3F
Source type:	Fertile	Fertile	Depleted	Depleted	Fertile	Fertile
Source wt % FeO:	8·0	8·0	8·0	8·0	9·0	9·0
Melting mechanism:	EQ	APFM	EQ	APFM	EQ	APFM
SiO_2	46·4	46·9	46·6	46·8	47·1	47·5
TiO_2	1·20	1·29	1·24	1·29	1·34	1·42
Al_2O_3	10·7	11·6	11·1	11·5	12·0	12·8
Cr_2O_3	0·05	0·05	0·05	0·05	0·05	0·06
Fe_2O_3	1·68	1·82	1·75	1·81	1·89	2·01
FeO	9·4	9·4	9·4	9·4	9·4	9·4
MnO	0·20	0·21	0·20	0·21	0·21	0·21
MgO	19·6	17·1	18·4	17·2	15·8	13·8
CaO	9·2	9·9	9·6	9·9	10·3	11·0
Na_2O	1·44	1·56	1·50	1·55	1·62	1·72
K_2O	0·08	0·09	0·09	0·09	0·09	0·10
NiO	0·111	0·081	0·096	0·083	0·067	0·048
Olivine *mg*-no.	91·5(0·4)	90·5(0·5)	91·1(0·5)	90·6(0·5)	89·9(0·5)	88·8(0·6)
F (melt fraction)	0·28	0·26	0·11	0·10	0·24	0·20
P (GPa)	3·2	3·3	2·8	n.d.	1·9	n.d.
T @ 4·0 GPa (°C)	1623	1580	1602	1582	1556	1516
T @ 1 atm (°C)	1439	1396	1418	1398	1372	1332

Olivine addition to sample 113325 (Holm *et al.*, 1993). Abbreviations and explanation as for Table 4.

8 on the *Journal of Petrology* Web site at http://www.petrology.oupjournals.org. Primary magmas for both fertile and depleted peridotite sources are restricted to 11·8–12·9% MgO, melt fractions range from 0·05 to 0·10, and computed olivines have *mg*-numbers of 89·9–90·5 (Table 8). The Siqueiros primary magma has somewhat more MgO and less FeO than those of N-MORB estimated by McKenzie and coworkers (McKenzie & Bickle, 1988; McKenzie & O'Nions, 1991; White *et al.*, 1992), differences that are discussed in Electronic Appendix 8. Olivines that precipitate from perfect fractional melts or olivine wall-rock xenocrysts from the melting regime are expected to have *mg*-numbers no higher than about 90·8 (Fig. 7b). Observed olivine phenocrysts contain *mg*-numbers of 89·5–91·5. The effect of a $\pm 1\sigma$ uncertainty in $K_D^{Ol/L}{}_{FeO/MgO}$ propagates to $\pm 0{\cdot}5$ in olivine *mg*-number, indicating a complex origin for $Ol_{91\text{-}5}$ observed in the lava flows. Indeed, Perfit *et al.* (1996) reported the the more magnesian grains show resorption and some of the larger more anhedral grains show deformation lamellae. Some melt inclusions in the olivine phenocrysts are unusual for MORB, and have been interpreted as examples of assimilated gabbroic cumulates + trapped liquid (L. V. Danyushevsky, personal communication, 2002). As many gabbroic cumulates are low in FeO, assimilation can potentially elevate the *mg*-number of the liquid and olivine precipitates. Localized crustal assimilation might explain why our computed olivine *mg*-numbers are somewhat lower than those in phenocrysts.

PLUME THERMAL AND PETROLOGICAL STRUCTURE

Primary magma temperatures have been calculated with equation (30) for liquids in equilibrium with olivine. Results have been provided in Tables 4–8 at 1 atm and 4 GPa. The MgO content of the liquid has the most important effect on olivine–liquid equilibration temperature, and other oxide components have significantly lesser effects. The olivine–liquid equilibration temperature of a primary magma with a specific MgO content is therefore very similar to that for a liquid in equilibrium with fertile or depleted mantle peridotite at the same MgO content. And as the MgO contents of primary magmas do not change significantly during decompression melting (Fig. 8a), we can use the MgO contents of liquids in equilibrium with mantle peridotite

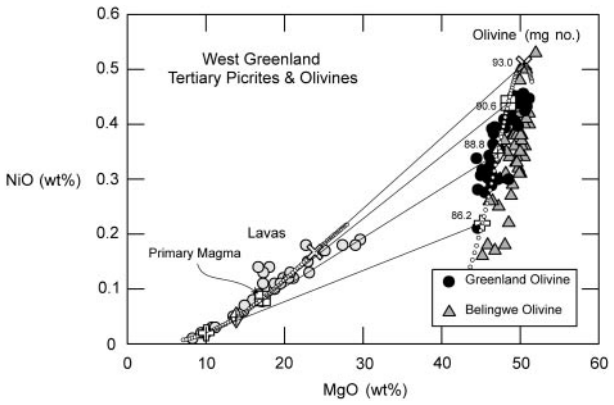

Fig. 12. NiO and MgO contents of lavas and olivines from West Greenland (Holm *et al.*, 1993) compared with calculated primary magmas produced by accumulated fractional melting and their olivine phenocrysts. Cross at 10% MgO for which olivine was added (small circles) is sample 113325 from West Greenland (Holm *et al.*, 1993); cross-in-square, primary magma for depleted peridotite source (Table 7; this is almost identical to primary magma for fertile peridotite source); open diamond, primary magma for Fe-rich peridotite source; open square, primary magma for depleted source; cross, lava composition in equilibrium with olivine with *mg*-number 93·0; grey filled circles, lavas from West Greenland (Holm *et al.*, 1993). Calculated olivine compositions are indicated with *mg*-numbers; tie lines tie together calculated olivine and primary magma compositions. Black filled circles, olivines in picrites from West Greenland (Larsen & Pedersen, 2000); grey filled triangles, olivines in Archaean komatiites from Belingwe (Renner *et al.*, 1994). Belingwe lava compositions are not shown for clarity, but their NiO contents are similar to those for Greenland lavas at any specific value of MgO.

Table 8: Calculated primary magma compositions for MORB from the Siqueiros transform fault (wt %)

	1E	1F	2E	2F
Source type:	Fertile	Fertile	Depleted	Depleted
Source wt % FeO:	8·0	8·0	8·0	8·0
Melting mechanism:	EQ	APFM	EQ	APFM
SiO_2	48·5	48·60	48·4	48·4
TiO_2	0·85	0·86	0·83	0·84
Al_2O_3	16·6	16·8	16·3	16·4
Cr_2O_3	n.d.	n.d.	n.d.	n.d.
Fe_2O_3	0·57	0·57	0·55	0·56
FeO	7·4	7·4	7·4	7·40
MnO	0·12	0·12	0·12	0·12
MgO	12·1	11·8	12·9	12·7
CaO	11·5	11·6	11·3	11·3
Na_2O	2·28	2·30	2·24	2·25
K_2O	n.d.	n.d.	n.d.	n.d.
NiO	n.d.	n.d.	n.d.	n.d.
Olivine *mg*-no.	90·1(0·5)	89·9(0·5)	90·5(0·5)	90·4(0·5)
F (melt fraction)	0·10	0·09	0·05	0·05
P (GPa)	1·4	2·0	1·5	n.d.
T @ 1 atm (°C)	1284	1277	1301	1297

Olivine addition to sample ALV2384-007B (Perfit *et al.*, 1996). Abbreviations and explanation as for Table 4.

as a proxy for the decompression melting *T*–*P* path. These are shown in Fig. 13.

The intersection of the decompression melting *T*–*P* path with the anhydrous solidus can place constraints on the thermal characteristics of the melting regime as defined by the potential temperature (T_p; McKenzie & Bickle, 1988) and the pressure of initial melting on the anhydrous solidus (i.e. P_o). For the case of a primary MORB magma having 12% MgO (Table 8), the eruption temperature is about 1275°C, P_o = 2·5 GPa and T_p = 1380°C (Fig. 13). These conditions are similar to those inferred by Asimow *et al.* (2001) for the production of 7 km of oceanic crust, but they are hotter than the 1300°C potential temperatures preferred by McKenzie and co-workers (McKenzie & Bickle, 1988; McKenzie & O'Nions, 1991; White *et al.*, 1992; Electronic Appendices 8 and 9 on the *Journal of Petrology* Web site at http://www.petrology.oupjournals.org). Primary magmas from Hawaii, Gorgona, Baffin Island and West Greenland with 18–20% MgO have eruption temperatures of about 1400–1440°C, intersect the solidus for fertile peridotite at 3·8–4·7 GPa (Fig. 13), and have potential temperatures of 1520–1570°C.

For Gorgona primary picrites with about 24% MgO we obtain P_o = 8·0 GPa, T_p = 1700°C, similar to those inferred by Thompson & Gibson (2000). However, the MgO content is not well constrained for fractional melts in equilibrium with $Ol_{93·6}$, and it can range from 23 to 26% (Fig. 11). When the MgO content of a primary fractional melt exceeds about 24% there can be very large uncertainties in both pressure of initial melting and the potential temperature because $\partial T/\partial P$ for isopleths for MgO are nearly parallel to those for the solidus (Fig. 13). Similarly, changes in peridotite source composition can affect solidus absolute temperature and estimates of initial melting pressures (Electronic Appendix 9), although detailed experimental calibrations are lacking. These problems can have important consequences for interpretations of Archaean komatiites with 20–30% MgO, a discussion is that is well beyond the scope of this paper.

Pressures of melting can be significantly deeper than lithosphere thickness (Fig. 13), consistent with the plume model. The formation of hotspots by shallow passive melting in response to stresses and cracks in the lithosphere is an important alternative (Anderson, 2000), but it is not consistent with topography on the 410 and 660

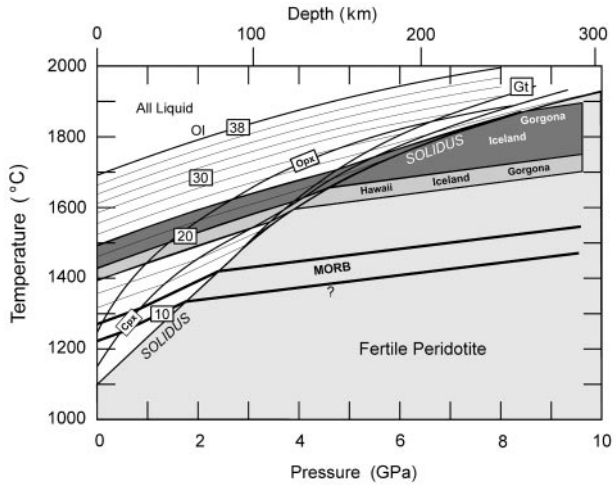

Fig. 13. A thermal model of adiabatic *T*–*P* paths for primary magmas with 12–24% MgO. Model adiabatic paths are coincident with isopleths of MgO in liquids formed by equilibrium melting of fertile peridotite (see text for discussion). Most plume-related primary magmas produced by accumulated fractional melting contain 18–20% MgO (Tables 4–7) for peridotite sources with about 8·0% FeO. Primary MORB from the Siqueiros transform fault contain about 12% MgO (Table 8). Olivine phenocrysts or wall-rock xenocrysts with *mg*-numbers of 93·0–93·6 are associated with Gorgona picrites and lavas from Baffin Island and West Greenland from the early Tertiary Icelandic plume. Uncertainties in MORB potential temperature are discussed in Electronic Appendices 8 and 9.

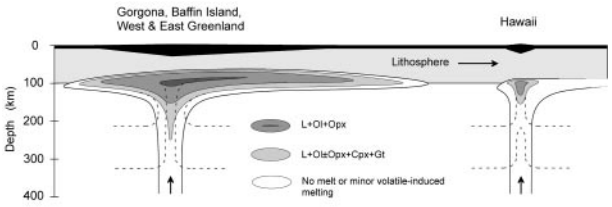

Fig. 14. A petrological model of plume structures, modified from Herzberg & O'Hara (1998). Left, plume head + axis model for the Gorgona and Icelandic plumes; right, plume axis model for Hawaii. Dark-coloured plume interior corresponds to high-temperature adiabatic gradients in Fig. 13, and is a region of advanced fractional melts in equilibrium with olivines with *mg*-numbers of 93·0–93·6. Broken lines are isotherms. Black region represents crust.

km discontinuities below Hawaii and Iceland (Shen *et al.*, 1998; Li *et al.*, 2000).

Picrites from Baffin Island and West Greenland occupy the western peripheral edge of eruption sites with 58–62 Ma ages scattered over 2000 km of the North Atlantic Igneous Province (White & McKenzie, 1989; Saunders *et al.*, 1997), a distribution that White & McKenzie (1989) related to the ancestral Icelandic plume. Computed plume simulations show considerable flattening of a plume head as it impacts the lithosphere, and that the plume head can stay hot over large horizontal distances (Larsen *et al.*, 1999). Picrites and basalts from the British Tertiary Igneous Province are also likely to have been extracted from the eastern Icelandic plume periphery. Many are olivine-phyric lavas with FeO_T contents that are higher than those for normal MORB (i.e. 10–13% FeO_T; Scarrow *et al.*, 2000), and they have elevated $^3He/^4He$ (Stuart *et al.*, 2000). Similarly, the distribution of 88–90 Ma komatiite and picritic lavas throughout the Caribbean–Colombian plateau has been interpreted as eruption from a large plume head (Kerr *et al.*, 1997). Our preferred model, shown in Fig. 14, has ultramafic magma production distributed throughout a large plume head within which liquids are extracted from a harzburgite residue (Herzberg & O'Hara, 1998), whereas it is restricted to the plume axis in the models of Campbell *et al.* (1989) and Campbell & Griffiths (1990).

Model petrological plume structures are shown in Fig. 14. Both plume heads and axes can consist of a harzburgite core [L + Ol + Opx] and a garnet peridotite periphery [L + Ol ± Opx + Cpx + Gt] (Eggins, 1992*b*; Herzberg & O'Hara, 1998). The Gorgona and early Tertiary Icelandic plumes differ from Hawaii in consisting of more head than tail. They also had a deeper and hotter plume core that contained advanced fractional melts in equilibrium with olivines having *mg*-numbers of 93·0–93·6. Fractional melts from the plume core may not have mixed with fractional melts from the plume periphery if melt percolation streamlines were dominantly vertical. Indeed, isotopic heterogeneity observed in individual shield volcanoes in Hawaii (Lassiter & Hauri, 1998; Blichert-Toft *et al.*, 1999) indicates that lateral melt movement is not signficant in a plume axis. The situation may be complex when material in the axis feeds a flattened plume head as it impacts the lithosphere (Fig. 14).

CONCLUSIONS

A parameterization of a large experimental database provides forward models of potential primary magma compositions that exit the melting regime in the mantle, and these are represented in CMAS projections and plots of FeO–MgO. The effects of equilibrium melting, fractional melting and peridotite source composition on FeO and MgO contents of potential primary magmas have been evaluated. The parameterization can also be used in inverse models for computing the effects of olivine fractionation for any olivine-phyric lava suite. A hybrid forward and inverse model provides a unique primary magma composition, eruption temperature, melt fraction and residuum mineralogy for any assumed peridotite source composition and melting mechanism.

The major element geochemistry of primary magmas from Gorgona, Hawaii, Baffin Island and West Greenland cannot be used to infer major element composition

of the source. The MgO contents of primary magmas are typically 18–20% MgO for wide variations in assumed fertile and depleted peridotite source compositions, and we estimate in Electronic Appendix 10 on the *Journal of Petrology* Web site (http://www.petrology.oupjournals.org) an uncertainty of $\pm 1\%$ MgO at the 1σ level of confidence. However, MgO can drop to 14–17% for Fe-enriched sources, and increase to 26% for fractional melts from Gorgona. One serious geological casualty is the large uncertainty in crustal thickness because different source compositions predict melt fractions that range from about 0·1 to 0·4. Another casualty is the large uncertainty in estimates of the pressure of melt collection (Electronic Appendix 10).

There is a substantial drop in the FeO content of both fractional melts and accumulated fractional melts during adiabatic decompression melting. However, there is little change in MgO because adiabatic *T*–*P* paths are nearly coincident with olivine–liquid *T*–*P* saturation surfaces. Olivine–liquid equilibrium temperatures therefore closely reflect actual eruption temperatures and adiabatic decompression melting paths.

Primary magmas from Hawaii, Gorgona, Baffin Island and West Greenland with 18–20% MgO have eruption temperatures of 1400–1440°C, intersect the solidus for an assumed fertile peridotite composition at 3·8–4·7 GPa, and have potential temperatures of 1520–1570°C. For Gorgona picrites with 24% MgO, the potential temperature and initial melting pressure were about 1700°C and 8·0 GPa, respectively; melting was hot and deep, consistent with the plume model.

Our work provides strong support for the importance of fractional melting in plumes (Arndt *et al.*, 1997). Primary magma compositions that we infer for accumulated fractional melting are in equilibrium with olivines with *mg*-numbers that are typically around 90·6, similar to observed maximum *mg*-numbers of olivines in lavas. Olivines with *mg*-numbers of 93·0–93·6 in lavas from Gorgona, Baffin Island and West Greenland could not have precipitated as phenocrysts from accumulated fractional melts or from equilibrium melts. Instead, they could have been in equilibrium with isolated advanced fractional melts having low FeO contents and MgO contents that are poorly constrained. In general, olivines with *mg*-numbers of 93·0–93·6 may be phenocrysts of perfect fractional melts that exited the melting regime or they may be wall-rock xenocrysts from the refractory plume core. The occurrence of olivines in lava flows with compositions that are expected from both well-mixed aggregate fractional melts and advanced fractional melts indicates that magma mixing in the melting regime of mantle plumes does not always occur, a conclusion reached independently by Slater *et al.* (2001) for Iceland.

The picrites from Gorgona are interpreted as advanced fractional melts that formed in the hot axis of a plume, a suggestion that was made previously by Arndt *et al.* (1997). Fractional melts with more than 24% MgO can have thermal characteristics that are difficult to constrain. A typical petrological plume structure consists of a harzburgite core [L + Ol + Opx] and a garnet peridotite periphery [L + Ol $\pm$ Opx + Cpx + Gt] located in both the head and axis.

ACKNOWLEDGEMENTS

We are very grateful to N. Arndt, P. Asimow, L. Larsen, R. N. Thompson and M. Wilson for thorough and constructive reviews.

REFERENCES

Aitken, B. G. & Echeverria, L. M. (1984). Petrology and geochemistry of komatiites and tholeiites from Gorgona Island, Colombia. *Contributions to Mineralogy and Petrology* **86**, 94–105.

Albarède, F. (1992). How deep do common basaltic magmas form and differentiate? *Journal of Geophysical Research* **97**, 10997–11009.

Anderson, D. L. (2000). The thermal state of the upper mantle; no role for mantle plumes. *Geophysical Research Letters* **27**, 3623–3626.

Arndt, N. T. (1986). Komatiites: a dirty window to the Archean mantle. *Terra Cognita* **6**, 59–66.

Arndt, N. T. & Nisbet, E. G. (1982). What is a komatiite? In: Arndt, N. T. & Nisbet, E. G. (eds) *Komatiites*. London: George Allen and Unwin, pp. 19–27.

Arndt, N. T., Kerr, A. C. & Tarney, J. (1997). Dynamic melting in plume heads: the formation of Gorgona komatiites and basalts. *Earth and Planetary Science Letters* **146**, 289–301.

Asimow, P. D., Hirschmann, M. M. & Stolper, E. M. (2001). Calculation of peridotite partial melting from thermodynamic models of minerals and melts, IV. Adiabatic decompression and the composition and mean properties of mid-ocean ridge basalts. *Journal of Petrology* **42**, 963–998.

Baker, M. B. & Beckett, J. R. (1999). The origin of abyssal peridotites: a reinterpretation of constraints based on primary bulk compositions. *Earth and Planetary Science Letters* **171**, 49–61.

Baker, M. B. & Stolper, E. M. (1994). Determining the composition of high-pressure mantle melts using diamond aggregates. *Geochimica et Cosmochimica Acta* **58**, 2811–2827.

Baker, M. B., Hirschmann, M. M., Ghiorso, M. S. & Stolper, E. M. (1995). Compositions of near-solidus peridotite melts from experiments and thermodynamic calculations. *Nature* **375**, 308–310.

Baker, M. B., Alves, S. & Stolper, E. M. (1996). Petrology of petrography of the Hawaii Scientific Drilling Project lavas: inferences from olivine phenocryst abundances and compositions. *Journal of Geophysical Research* **101**, 11715–11727.

Beattie, P. (1993). Olivine–melt and orthopyroxene–melt equilibria. *Contributions to Mineralogy and Petrology* **115**, 103–111.

Beattie, P., Ford, C. & Russell, D. (1991). Partition coefficients for olivine–melt and orthopyroxene–melt systems. *Contributions to Mineralogy and Petrology* **109**, 212–224.

Blichert-Toft, J., Frey, F. A. & Albarède, F. (1999). Hf isotope evidence for pelagic sediments in the source of Hawaiian basalts. *Science* **285**, 879–882.

Bowen, N. L. (1928). *The Evolution of the Igneous Rocks*. Princeton, NJ: Princeton University Press, 332 pp.

Campbell, I. H. & Griffiths, R. W. (1990). Implications of mantle plume structure for the evolution of flood basalts. *Earth and Planetary Science Letters* **99**, 79–93.

Campbell, I. H., Griffiths, R. W. & Hill, R. I. (1989). Melting in an Archaean mantle plume: heads it's basalts and tails it's komatiites. *Nature* **339**, 697–699.

Canil, D. (1999). Vanadium partitioning between orthopyroxene, spinel and silicate melt and the redox states of mantle source regions for primary magmas. *Geochimica et Cosmochimica Acta* **63**, 557–572.

Canil, D., O'Neill, H. St. C., Pearson, D. G., Rudnick, R. L., McDonough, W. F. & Carswell, D. A. (1994). Ferric iron in peridotites and mantle oxidation states. *Earth and Planetary Science Letters* **123**, 205–220.

Cawthorn, R. G. (1975). Degrees of melting in mantle diapirs and the origin of ultrabasic liquids. *Earth and Planetary Science Letters* **27**, 113–120.

Christie, D. M., Carmichael, I. S. E. & Langmuir, C. H. (1986). Oxidation states of mid-ocean ridge basalt glasses. *Earth and Planetary Science Letters* **79**, 397–411.

Clague, D. A., Weber, W. S. & Dixon, J. E. (1991). Picritic glasses from Hawaii. *Nature* **353**, 553–556.

Clarke, D. B. (1970). Tertiary basalts of Baffin Bay: possible primary magma from the mantle. *Contributions to Mineralogy and Petrology* **25**, 203–224.

Clarke, D. B. & O'Hara, M. J. (1979). Nickel, and the existence of high-MgO liquids in nature. *Earth and Planetary Science Letters* **44**, 153–158.

Clarke, D. B. & Pedersen, A. K. (1976). Tertiary volcanic province of Baffin Bay. In: Escher, A. & Watts, W. S. (eds) *Geology of Greenland*. Copenhagen: Geological Survey of Greenland, pp. 365–385.

Danyushevsky, L. V. & Sobolev, A. V. (1996). Ferric–ferrous ratio and oxygen fugacity calculations for primitive mantle-derived melts: calibration of an empirical technique. *Mineralogy and Petrology* **57**, 229–241.

Drever, H. I. (1956). The geology of Ubekendt Ejland, West Greenland, Part II. *Meddelelser Om Grønland* **137**, 1–39.

Drever, H. I. & Johnston, R. (1957). Crystal growth of forsteritic olivine in magmas and melts. *Transactions of the Royal Society of Edinburgh* **63**, 289–315.

Echeverria, L. M. (1980). Tertiary or Mesozoic komatiites from Gorgona Island, Colombia: field relations and geochemistry. *Contributions to Mineralogy and Petrology* **73**, 253–266.

Echeverria, L. M. & Aitken, B. G. (1986). Pyroclastic rocks: another manifestation of ultramafic volcanism on Gorgona Island, Colombia. *Contributions to Mineralogy and Petrology* **92**, 428–436.

Eggins, S. M. (1992*a*). Petrogenesis of Hawaiian tholeiites: 1, phase equilibria constraints. *Contributions to Mineralogy and Petrology* **110**, 387–397.

Eggins, S. M. (1992*b*). Petrogenesis of Hawaiian tholeiites: 2, aspects of dynamic melt segregation. *Contributions to Mineralogy and Petrology* **110**, 398–410.

Elthon, D. & Ridley, W. I. (1979). Comments on: 'The partitioning of nickel between olivine and silicate melt' by S. R. Hart and K. E. Davis. *Earth and Planetary Science Letters* **44**, 162–164.

Falloon, T. J., Green, D. H., Danyushevsky, L. V. & Faul, U. H. (1999*a*). Peridotite melting at 1·0 and 1·5 GPa: an experimental evaluation of techniques using diamond aggregates and mineral mixes for determination of near-solidus melts. *Journal of Petrology* **40**, 1343–1375.

Falloon, T. J., Green, D. H., Jacques, A. L. & Hawkins, J. W. (1999*b*). Refractory magmas in back-arc basin settings—experimental constraints on the petrogenesis of a Lau Basin example. *Journal of Petrology* **40**, 255–277.

Feigenson, M. D. (1984). Geochemistry of Kauai volcanics and a mixing model for the origin of Hawaiian alkali basalts. *Contributions to Mineralogy and Petrology* **87**, 109–119.

Francis, D. (1985). The Baffin Bay lavas and the value of picrites as analogues of primary magmas. *Contributions to Mineralogy and Petrology* **89**, 144–154.

Fyfe, W. S. (1978). The evolution of the Earth's crust: modern plate tectonics to ancient hot spot tectonics? *Chemical Geology* **23**, 89–114.

Gast, P. W. (1968). Trace element fractionation and the origin of tholeiitic and alkaline magma types. *Geochimica et Cosmochimica Acta* **32**, 1057–1086.

Gill, R. C. O., Pedersen, A. K. & Larsen, J. G. (1992). Tertiary picrites in West Greenland: melting at the periphery of a plume? In: Storey, B. C., Alabaster, T. & Pankhurst, R. J. (eds) *Magmatism and the Causes of Continental Break-up. Geological Society, London, Special Publications* **68**, 335–348.

Griffin, W. L., O'Reilly, S. Y. & Ryan, C. G. (1999). The composition and origin of sub-continental lithospheric mantle. In: Fei, Y., Bertka, C. M. & Mysen, B. O. (eds) *Mantle Petrology: Field Observations and High Pressure Experimentation. A Tribute to Francis R. (Joe) Boyd. Geochemical Society, Special Publication* **6**, 13–45.

Gudfinnson, G. H. & Presnall, D. C. (2000). Melting behaviour of model lherzolite in the system CaO–MgO–Al_2O_3–SiO_2–FeO at 0·7–2·8 GPa. *Journal of Petrology* **41**, 1241–1269.

Hart, S. R. & Davis, K. E. (1978). Nickel partitioning between olivine and silicate melt. *Earth and Planetary Science Letters* **40**, 203–219.

Hauri, E. (1996). Major-element variability in the Hawaiian mantle plume. *Nature* **382**, 415–419.

Herzberg, C. T. (1992). Depth and degree of melting of komatiites. *Journal of Geophysical Research* **97**, 4521–4540.

Herzberg, C. T. (1993). Lithosphere peridotites of the Kaapvaal craton. *Earth and Planetary Science Letters* **120**, 13–29.

Herzberg, C. & O'Hara, M. J. (1998). Phase equilibrium constraints on the origin of basalts, picrites, and komatiites. *Earth-Science Reviews* **44**, 39–79.

Herzberg, C. & Zhang, J. (1996). Melting experiments on anhydrous peridotite KLB-1: compositions of magmas in the upper mantle and transition zone. *Journal of Geophysical Research* **101**, 8271–8295.

Herzberg, C. & Zhang, J. (1998). Melting experiments in the systems CaO–MgO–Al_2O_3–SiO_2 and MgO–SiO_2 at 3 to 15 GPa. *American Mineralogist* **83**, 491–500.

Herzberg, C., Raterron, P. & Zhang, J. (2000). New experimental observations on the anhydrous solidus for peridotite KLB-1. *Geochemistry, Geophysics, Geosystems* **1**, 2000GC000089.

Hirose, E. & Kushiro, I. (1993). Partial melting of dry peridotites at high pressures: determination of compositions of melts segregated from peridotite using aggregates of diamond. *Earth and Planetary Science Letters* **114**, 477–489.

Hirschmann, M. M. (2000). Mantle solidus: experimental constraints and the effects of peridotite composition. *Geochemistry, Geophysics, Geosystems* **1**, 2000GC000070.

Hirschmann, M. M. & Ghiorso, M. S. (1994). Activities of nickel, cobalt, and manganese silicates in magmatic liquids and applications to olivine/liquid and to silicate/metal partitioning. *Geochimica et Cosmochimica Acta* **58**, 4109–4126.

Hirschmann, M. M., Baker, M. B. & Stolper, E. M. (1998). The effect of alkalis on the silica content of mantle-derived melts. *Geochimica et Cosmochimica Acta* **62**, 883–902.

Holm, P. M., Gill, R. C. O., Pedersen, A. K., Larsen, J. G., Hald, N., Nielsen, T. F. D. & Thirlwall, M. F. (1993). The Tertiary picrites of West Greenland: contributions from 'Icelandic' and other sources. *Earth and Planetary Science Letters* **115**, 227–244.

Iwamori, H., McKenzie, D. & Takahashi, E. (1995). Melt generation by isentropic mantle upwelling. *Earth and Planetary Science Letters* **134**, 253–266.

Jakobsson, S. P., Jónsson, J. & Shido, F. (1978). Petrology of the Western Reykjanes Peninsula, Iceland. *Journal of Petrology* **19**, 669–705.

Jarvis, G. T. & Campbell, I. H. (1983). Archean komatiites and geotherms: solution to an apparent contradiction. *Geophysical Research Letters* **10**, 1133–1136.

Jones, J. H. (1995). Experimental trace element partitioning. In: Ahrens, T. J. (ed.) *Rock Physics and Phase Relations. AGU Handbook of Physical Constants 3*. Washington, DC: American Geophysical Union, pp. 73–104.

Kerr, A. C. & Arndt, N. T. (2001). A note on the IUGS reclassification of the high-Mg and picritic volcanic rocks. *Journal of Petrology* **42**, 2169–2171.

Kerr, A. C., Marriner, G. F., Arndt, N. T., Tarney, J., Nivia, A., Saunders, A. D. & Duncan, R. A. (1996). The petrogenesis of Gorgona komatiites, picrites and basalts: new field, petrographic and geochemical constraints. *Lithos* **37**, 245–260.

Kerr, A. C., Tarney, J., Marriner, G. F., Nivia, A. & Saunders, A. D. (1997). The Caribbean–Colombian Cretaceous igneous province: the internal anatomy of an oceanic plateau. In: Mahoney, J. J. & Coffin, M. L. (eds) *Large Igneous Provinces. Geophysical Monograph, American Geophysical Union* **100**, 123–144.

Kilinc, A., Carmichael, I. S. E., Rivers, M. L. & Sack, R. O. (1983). The ferric–ferrous ratio of natural silicate liquids equilibrated in air. *Contributions to Mineralogy and Petrology* **83**, 136–140.

Kinzler, R. (1997). Melting of mantle peridotite at pressures approaching the spinel to garnet transition: application to mid-ocean ridge basalt petrogenesis. *Journal of Geophysical Research* **102**, 853–874.

Kress, V. C. & Carmichael, I. S. E. (1991). The compressibility of silicate liquids containing Fe_2O_3 and the effect of composition, temperature, oxygen fugacity and pressure on their redox states. *Contributions to Mineralogy and Petrology* **108**, 82–92.

Kushiro, I. (1996). Partial melting of a fertile mantle peridotite at high pressures: an experimental study using aggregates of diamond. In: Basu, A. & Hart, S. (eds) *Earth Processes: Reading the Isotopic Code. Geophysical Monograph, American Geophysical Union* **95**, 109–122.

Langmuir, C. H., Klein, E. M. & Plank, T. (1992). Petrology systematics of mid-ocean ridge basalts: constraints on melt generation beneath ocean ridges. In Morgan, J. P., Blackman, D. K., Sinton, J. M. (eds), *Mantle Flow and Melt Generation at Mid-Ocean Ridges. Geophysical Monograph, American Geophysical Union* **71**, 183–280.

Larsen, L. M. & Pedersen, A. K. (2000). Processes in high-Mg, high-*T* magmas: evidence from olivine, chromite and glass in Palaeogene picrites from West Greenland. *Journal of Petrology* **41**, 1071–1098.

Larsen, L. M., Pedersen, A. K., Pedersen, G. K. & Piasecki, S. (1992). Timing and duration of Early Tertiary volcanism in the North Atlantic: new evidence from West Greenland. In: Storey, B. C., Alabaster, T. & Pankhurst, R. J. (eds) *Magmatism and the Causes of Continental Break-up. Geological Society, London, Special Publications* **68**, 321–333.

Larsen, T. B., Yuen, D. A. & Storey, M. (1999). Ultrafast mantle plumes and implications for flood basalt volcanism in the Northern Atlantic region. *Tectonophysics* **311**, 31–43.

Lassiter, J. C. & Hauri, E. H. (1998). Osmium-isotope variations in Hawaiian lavas: evidence for recycled oceanic lithosphere in the Hawaiian plume. *Earth and Planetary Science Letters* **164**, 483–496.

Le Bas, M. J. (2000). IUGS reclassification of the high-Mg and picritic volcanic rocks. *Journal of Petrology* **41**, 1467–1470.

Le Bas, M. J. (2001). Reply to comment by Kerr and Arndt. *Journal of Petrology* **42**, 2173–2174.

Li, X., Kind, R., Priestley, K., Sobolov, S. V., Tilmann, F., Yuan, X. & Weber, M. (2000). Mapping the Hawaiian plume conduit with converted seismic waves. *Nature* **405**, 938–941.

Longhi, J. (1995). Liquidus equilibria of some primary lunar and terrestrial melts in the garnet stability field. *Geochimica et Cosmochimica Acta* **59**, 2375–2386.

McKenzie, D. & Bickle, M. J. (1988). The volume and composition of melt generated by extension of the lithosphere. *Journal of Petrology* **29**, 625–679.

McKenzie, D. & O'Nions, R. K. (1991). Partial melt distributions from inversion of rare-earth element concentrations. *Journal of Petrology* **32**, 1021–1091.

Murata, K. J. & Richter, D. H. (1966). Chemistry of the lavas of the 1959–1960 eruption of Kilauea volcano, Hawaii. *US Geological Survey Professional Paper* **537-A**, 1–26.

Nisbet, E. G., Cheadle, M. J., Arndt, N. T. & Bickle, M. J. (1993). Constraining the potential temperature of the Archaean mantle: a review of the evidence from komatiites. *Lithos* **30**, 291–307.

Norman, M. D. & Garcia, M. O. (1999). Primitive magmas and source characteristics of the Hawaiian plume: petrology and geochemistry of shield picrites. *Earth and Planetary Science Letters* **168**, 27–44.

O'Hara, M. J. (1968*a*). The bearing of phase equilibria studies in synthetic and natural systems on the origin of basic and ultrabasic rocks. *Earth-Science Reviews* **4**, 69–133.

O'Hara, M. J. (1968*b*). Are ocean floor basalts primary magmas? *Nature* **220**, 683–686.

O'Hara, M. J. & Herzberg, C. (2002). Interpretation of trace element and isotope features of basalts: relevance of field relations, petrology, major element data, phase equilibria and magma chamber modelling in basalt petrogenesis. *Geochimica et Cosmochimica Acta*, **66**, 2167–2191.

O'Hara, M. J., Richardson, S. W. & Wilson, G. (1971). Garnet-peridotite stability and occurrence in crust and mantle. *Contributions to Mineralogy and Petrology* **32**, 48–68.

O'Neill, H. St. C. (1987). Quartz–fayalite–iron and quartz–fayalite–magnetite equilibria and the free energy of formation of fayalite (Fe_2SiO_4) and magnetite (Fe_3O_4). *American Mineralogist* **72**, 67–75.

O'Neill, H. St. C. & Pownceby, M. I. (1993). Thermodynamic data from redox reactions at high temperatures. I. An experimental and theoretical assessment of the electrochemical method using stabilized zirconia electrolytes, with revised values for the Fe–'FeO', Co–CoO, Ni–NiO and Cu–Cu_2O oxygen buffers, and new data for the W–WO_2 buffer. *Contributions to Mineralogy and Petrology* **114**, 296–314.

Pedersen, A. K. (1985). Reaction between picrite magma and continental crust: early Tertiary silicic basalts and magnesian andesites from Disko, West Greenland. *Bulletin Grønlands Geologiske Undersøgelse* **152**, 126 pp.

Perfit, M. R., Fornari, D. J., Ridley, W. I., Kirk, P. D., Casey, J., Kastens, K. A., Reynolds, J. R., Edwards, M., Desonie, D., Shuster, R. & Paradis, S. (1996). Recent volcanism in the Siqueiros transform fault: picritic basalts and implications for MORB magma genesis. *Earth and Planetary Science Letters* **141**, 91–108.

Putirka, K. (1999). Melting depths and mantle heterogeneity beneath Hawaii and the East Pacific Rise: constraints from Na/Ti and rare earth element ratios. *Journal of Geophysical Research* **104**, 2817–2829.

Renner, R., Nisbet, E. G., Cheadle, M. J., Arndt, N. T., Bickle, M. J. & Cameron, W. E. (1994). Komatiite flows from the Reliance Formation, Belingwe Belt, Zimbabwe: I. Petrography and mineralogy. *Journal of Petrology* **35**, 361–400.

Révillon, S., Arndt, N. T., Chauvel, C. & Hallot, E. (2000). Geochemical study of ultramafic volcanic and plutonic rocks from Gorgona Island, Colombia: the plumbing system of an oceanic plateau. *Journal of Petrology* **41**, 1127–1153.

Robillard, I., Francis, D. & Ludden, J. N. (1992). The relationship between E- and N-type magmas in the Baffin Bay Lavas. *Contributions to Mineralogy and Petrology* **112**, 230–241.

Roeder, P. L. & Emslie, R. F. (1970). Olivine–liquid equilibrium. *Contributions to Mineralogy and Petrology* **29**, 275–289.

Saunders, A. D., Fitton, J. G., Kerr, A. C., Norry, M. J. & Kent, R. W. (1997). The North Atlantic Igneous Province. In: Mahoney, J. J. & Coffin, M. L. (eds) *Large Igneous Provinces. Geophysical Monograph, American Geophysical Union* **100**, 45–93.

Scarrow, J. H., Curran, J. M. & Kerr, A. C. (2000). Major element records of variable plume involvement in the North Atlantic Province Tertiary flood basalts. *Journal of Petrology* **41**, 1155–1176.

Sims, K. W. W., DePaolo, D. J., Murrell, M. T., Baldridge, W. S., Goldstein, S. Clague, D. & Jull, M. (1999). Porosity of the melting zone and variations in the solid mantle upwelling rate beneath Hawaii: inferences from ^{238}U–^{230}Th–^{226}Ra and ^{235}U–^{231}Pa disequilibria. *Geochimica et Cosmochimica Acta* **63**, 4119–4138.

Shaw, D. M. (1970). Trace element fractionation during anatexis. *Geochimica et Cosmochimica Acta* **34**, 237–243.

Shen, Y., Solomon, S. C., Bjarnason, I. Th. & Wolfe, C. J. (1998). Seismic evidence for a lower-mantle origin of the Iceland plume. *Nature* **395**, 62–65.

Slater, L., McKenzie, D., Grönvold, K. & Shimizu, N. (2001). Melt generation and movement beneath Theistareykir, NE Iceland. *Journal of Petrology* **42**, 321–354.

Smith, D. & Boyd, F. R. (1987). Compositional heterogeneities in a high-temperature lherzolite nodule and implications for mantle processes. In: Nixon, P. H. (ed.) *Mantle Xenoliths*. New York: Wiley, pp. 551–561.

Sobolev, A. V. & Danyushevsky, L. V. (1994). Petrology and geochemistry of boninites from the North Termination of the Tonga Trench: constraints on the generation conditions of primary high-Ca boninite magmas. *Journal of Petrology* **35**, 1183–1211.

Stracke, A., Salters, V. J. M. & Sims, K. W. W. (1999). Assessing the presence of garnet-pyroxenite in the mantle sources of basalts through combined hafnium–neodymium–thorium isotope systematics. *Geochemistry, Geophysics, Geosystems* **1**, 1999GC000013.

Stuart, F. M., Ellam, R. M., Harrop, P. J., Fitton, J. G. & Bell, B. R. (2000). Constraints on mantle plumes from the helium isotopic composition of basalts from the British Tertiary Igneous Province. *Earth and Planetary Science Letters* **177**, 273–285.

Takahashi, E. & Kushiro, I. (1983). Melting of a dry peridotite at high pressures and basalt genesis. *American Mineralogist* **68**, 859–879.

Thompson, R. N. & Gibson, S. A. (2000). Transient high temperatures in mantle plume heads inferred from magnesian olivines in Phanerozoic picrites. *Nature* **407**, 502–506.

Ulmer, P. (1989). The dependence of the Fe^{2+}–Mg cation-partitioning between olivine and basaltic liquid on pressure, temperature and composition. An experimental study to 30 kbars. *Contributions to Mineralogy and Petrology* **101**, 261–273.

Walter, M. J. (1998). Melting of garnet peridotite and the origin of komatiite and depleted lithosphere. *Journal of Petrology* **39**, 29–60.

White, R. S. & McKenzie, D. (1989). Magmatism at rift zones: the generation of volcanic continental margins and flood basalts. *Journal of Geophysical Research* **94**, 7685–7729.

White, R. S., McKenzie, D. & O'Nions, R. K. (1992). Oceanic crustal thickness from seismic measurements and rare earth element inversions. *Journal of Geophysical Research* **97**, 19683–19715.

Wright, T. (1972). Chemistry of Kilauea and Mauna Loa lava in space and time. *US Geological Survey Professional Paper* **735**, 1–39.

Wright, T. (1973). Magma mixing as illustrated by the 1959 eruption, Kilauea Volcano, Hawaii. *Geological Society of America Bulletin* **84**, 849–858.

Wright, T. & Fiske, R. S. (1971). Origin of the differentiated and hybrid lavas of Kilauea Volcano, Hawaii. *Journal of Petrology* **12**, 1–65.

Wright, T., Swanson, D. A. & Duffield, W. A. (1975). Chemical compositions of Kilauea east-rift lava, 1968–1971. *Journal of Petrology* **16**, 110–133.

Xue, X., Baadsgaard, H., Irving, A. J. & Scarfe, C. M. (1990). Geochemical and isotopic characteristics of lithosphere mantle beneath West Kettle River, British Columbia: evidence from ultramafic xenoliths. *Journal of Geophysical Research* **95**, 15879–15891.

Yaxley, G. M. (2000). Experimental study of the phase and melting relations of homogeneous basalt + peridotite mixtures and implications for the petrogenesis of flood basalts. *Contributions to Mineralogy and Petrology* **139**, 326–338.